PHONON INTENSITY ANOMALIES IN YTTRIUM BARIUM COPPER OXIDE

by

Xiaojun Zhao

B.Eng. Tsinghua University (Beijing, China),1983

M.Eng. Tsinghua University (Beijing, China),1986

THESIS SUBMITTED IN PARTIAL FULFILLMENT OF THE REQUIREMENTS FOR THE DEGREE OF MASTER OF SCIENCE

in the Department

of

Physics

Simon Fraser University

March. 1994

ISBN 0-612-00996-3

Approval

Name : Xiaojun Zhao

Degree : Master of Science

Title of Thesis : Phonon Intensity Anomalies in $YBa_2Cu_3O_{7-x}$

Examining Committee:

Chairman : Dr. J.Dahn

Dr. J.C.Irwin
Senior Supervisor

Dr. E.D.Crozier

Dr. S.Gygax

Dr. H.J.Trodahl
External Examiner
Victoria University of Wellington
New Zealand

Date Approved : March 29, 1994

PARTIAL COPYRIGHT LICENSE

I hereby grant to Simon Fraser University the right to lend my thesis, project or extended essay (the title of which is shown below) to users of the Simon Fraser University Library, and to make partial or single copies only for such users or in response to a request from the library of any other university, or other educational institution, on its own behalf or for one of its users. I further agree that permission for multiple copying of this work for scholarly purposes may be granted by me or the Dean of Graduate Studies. It is understood that copying or publication of this work for financial gain shall not be allowed without my written permission.

Title of Thesis/Project/Extended Essay

PHONON INTENSITY ANOMALIES IN YTTRIUM BARIUM COPPER OXIDE

Author: _____
(signature)

XIAOJUN ZHAO
(name)

Mar 6, 1994
(date)

Abstract

The integrated Raman intensities of the A_{1g} and B_{1g} phonons in single crystals of $YBa_2Cu_3O_{7-x}$ with x = 0.00, 0.01 and 0.07 were measured in a near back scattering geometry as a function of temperature between 300K and 20K. The phonon intensities were normalized relative to the intensity of the Raman continuum in the region from 700cm^{-1} to 900cm^{-1}. When the samples were cooled to temperature below T_c, the intensity of the B_{1g} phonon at 340cm^{-1} exhibited the strongest effects. The normalized intensity of the B_{1g} phonon, in the sample with x = 0.00, began to rapidly increase at $T \leq T_c$ and by T = 20K the relative intensity had increased by a factor of 4±0.7. The effect was smaller in the sample with x = 0.07, with the enhancement factor being about 1.8±0.3 but with the onset still occurring near T_c. In the scattering geometry used in these experiments the only A_{1g} phonon that could be accurately measured was the vibration at 115cm^{-1}. In this case the normalized intensity was also enhanced below T_c with an onset temperature close to T_c and the measured enhancement factor was approximately 2±0.3 in all the samples.

The phonon intensity variations have been compared to other results obtained from Raman spectra and it is found that the temperature and doping dependence of the intensities is consistent with the picture implied by previous measurements of the phonon frequency and linewidth anomalies and electronic Raman continua. It is concluded that the intensity enhancements occur as a result of the resonance between the phonons and a gap that opens below T_c. It is speculated that the intensity enhancement of the A_{1g} phonons results from resonance with a d-wave superconducting gap while the B_{1g} phonon, because of the strong dependence on doping, might be attributed to resonance with excitations across a spin gap.

Acknowledgments

I appreciate the various help and advice that many people gave me in my work.

Special thanks go to Dr. X. Chen. He introduced me into the Raman scattering experiments step by step and has been giving me the encouragement and various help since then. He also passed some of his experimental data to me.

I also want to express my gratitude to Dr.S.Gygax, Dr.G.Soerensen and W.Xing for carrying out magnetic susceptibility measurements on the crystals and to Dr.J.Chrzanowski for his help.

Thanks go to Professor J. C. Irwin, my senior supervisor, for his continuous support and instructive supervision.

Thanks go to Simon Fraser University for the graduate fellowship that I received during the period of the work presented here.

Table of Contents

List of Figures

List of Tables

Chapter 1
Introduction

1.1 A Brief Review

Superconductivity was first discovered by Kamerlingh Onnes in mercury in 1911.[1] The transition temperature T_c , the critical temperature at which the dc resistivity of mercury dropped to zero, was 4.2K. Many kinds of materials, metallic elements, alloys and compounds, have now been found to be superconducting at sufficiently low temperatures.[2] Before 1986, the highest T_c observed was 23.2K in Nb_3Ge.[2] The physical mechanism responsible for superconductivity was first established by Bardeen, Cooper and Schrieffer in 1957, and is usually referred to as BCS theory.[3] In BCS theory, an effective attraction between electrons with energies around the Fermi energy is produced by the electron lattice interaction, the exchange of phonons between electrons. The brief physical picture is this: the motion of an electron polarizes the lattice, there is an effective attraction to another electron in the polarized region. The effective attraction leads to superconducting states which have lower energies than the Fermi energy. Each superconducting state is occupied by two electrons with the same energy, opposite momentum and opposite spin. For the materials in which superconductivity can be well described by BCS theory, the acoustic phonon energy as measured by the Debye temperature of the material determines the energy scale involved in the formation of the superconducting states. The transition temperatures of such materials are thus relatively low (< 20 K) and we usually call such superconductors the conventional superconductors.

In 1986, a superconducting transition near 30K in a heavily doped ceramic compound ($La_{1-x}Ba_xCuO_4$) was observed by A. Mueller and G. Bednorz.[4] Their discovery was the beginning of a new era of superconductivity and quickly led to the discovery of $YBa_2Cu_3O_7$ (Y123) with a transition temperature around 90K.[5] Now there have been many more superconducting materials discovered which are based on CuO_2 layers common to the two superconducting materials mentioned above. $Tl_2Ba_2Ca_2Cu_3O_{10}$ had the highest transition temperature, ~ 125K,[6] until the very recent discovery of the Hg based compounds which have produced a T_c near 133K.[7] In order to distinguish these superconducting materials from the conventional superconductors, we call them high-T_c superconductors or the unconventional superconductors. All the high T_c materials containing the CuO_2 layers have another feature in common: Their parent compounds are antiferromagnetic insulators. Upon doping, the long range antiferromagnetic order is destroyed and the materials become so-called strange metals whose resistivities in their normal phase are proportional to the temperature.[8] In a normal Fermi liquid, if the resistivity is limited by phonons, there exists a transition region between the high temperature region where the temperature T is greater than the Debye temperature (θ_D) and the resistivity is proportional to the temperature T and the low temperature region where $T << \theta_D$ and the resistivity is proportional to T^5.[9] For the high T_c superconductors, the Debye temperature is approximately in the region from 200 to 600K. In some high-T_c superconductors, the resistivity is proportional to T from just above T_c to several hundred Kelvins.[8] That is the transition

region mentioned above appears to be absent from some families of high T_c materials. This is definitely not a characteristic of the normal Fermi liquid. But the observation of the Fermi surfaces in high-T_c materials by angle resolved photon emission experiments[10] is consistent with normal Fermi liquid. One thing is clear that if normal Fermi liquid theory is applicable in principle in these high-T_c materials , some modifications are necessary to account for the normal state properties of these materials, such as the resistivity and the temperature dependence of the Hall coefficient.[8]

1.2 Raman Scattering from Superconductors

In the visible light region, Raman scattering can provide information about all the Raman active phonons which includes the frequency, the linewidth and the intensity for each phonon. If a Raman active phonon interacts strongly with the free carriers and has an energy close to the superconducting gap value, it can exhibit large superconductivity induced anomalies in its linewith, Raman shift and intensity. Raman scattering studies of these anomalies were used to obtain an estimate of $\frac{2\Delta}{k_b T_c} \approx 5.0$ for the superconducting gap 2Δ in polycrystalline samples with $T_c \sim 90K$.[11,12] The electronic Raman scattering can, on the other hand, provide information about the distribution of the electronic states at different temperatures.[13] This direct information can be used to verify the existence of the gap and to illustrate the symmetry property of the gap.[14-16]

1.2.1 Electronic Raman Scattering from Superconductors

In the normal state ($T > T_c$) of a typical metal, all the states above the Fermi energy are almost empty; all the states below the Fermi energy are almost fully occupied. Electronic Raman Scattering can only happen in a very small energy region around the Fermi energy. An electron with a wave vector $\mathbf{k}$ can be excited to a state $\mathbf{k'} = \mathbf{k} + \mathbf{q}$, where $\mathbf{q} = \mathbf{k_L} - \mathbf{k_S}$. $\mathbf{k_L}$ and $\mathbf{k_S}$ are the wave vectors of the incident and scattered photons respectively. For the visible light, $|\mathbf{q}| << |\mathbf{k_f}|$; $\mathbf{k_f}$ is a wave vector on the Fermi surface. The excitation energy $\hbar\omega$, when measured relative to the Fermi energy E_f, is

$$\hbar\omega = \frac{\hbar^2(\mathbf{k}+\mathbf{q})^2}{2m^*} - \frac{\hbar^2 k_f^2}{2m^*} \qquad 1\text{-}1$$

where m^* is the effective mass of an electron. The maximum of $\hbar\omega$ occurs for $|\mathbf{k}| \cong |\mathbf{k_f}|$ and

$$\omega_{max} = \frac{\hbar}{2m^*}(2\mathbf{q}\cdot\mathbf{k_f} + q^2) \quad . \qquad 1\text{-}2$$

If the q^2 term is neglected, we have $\omega_{max} = \frac{\hbar\mathbf{q}\cdot\mathbf{k_f}}{m^*} = \mathbf{q}\cdot\mathbf{v_f}$. v_f is the Fermi velocity.[13] Therefore in a normal metal there is a cutoff at the high energy end in the electronic Raman scattering spectra. An electronic Raman spectrum from free carriers in GaAs[13] is shown in Fig.1.1.

In a metal, the optical penetration depth δ is usually much less than the optical wavelength λ and in this case δ^{-1} is usually taken as a measure of the momentum transfer q. If in the superconducting state the penetration depth of

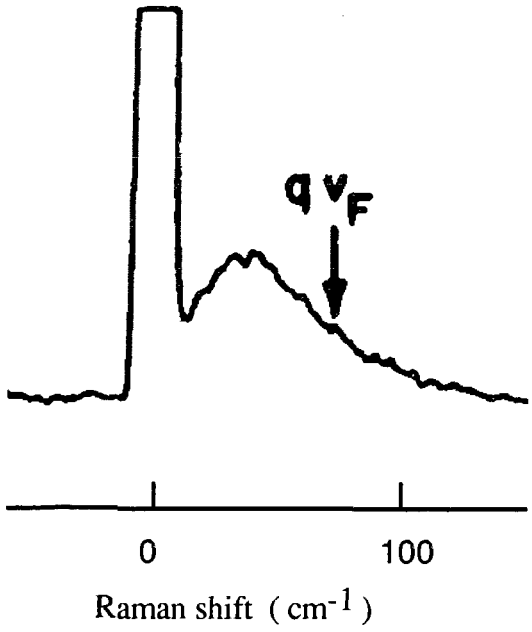

Figure 1.1 Illustration of Electornic Raman scattering in n-doped GaAs at 2K. (taken from Ref. 13) The strong peak at $\omega = 0$, which has been truncated, corresponds to elastic scatttering of the incident laser line.

the light δ is small compared with the coherence length ξ, where ξ is defined by $\xi = \hbar v_f(2\Delta)^{-1}$ and 2Δ is the superconducting gap value, one is in the limit[15] of large wave vector transfer $|\mathbf{q}|$. As is predicted in the theoretical calculation by M.V.Klein and S.B.Dierker[15] (Fig. 1.2 (a)), at zero temperature, the intensity of electronic Raman scattering turns on discontinuously at energy equal to 2Δ; as the energy increases, the scattering intensity increases very slowly and gradually returns to the normal state scattering intensity from above. There is no sharp peak feature in the low energy part of the electronic Raman spectra.

When the penetration depth of the light is larger than the coherence length, one has the so called $q \sim 0$ case or small wave vector transfer limit. In this small $|\mathbf{q}|$ limit,[15] as is shown in Fig. 1.2 (b) , a peak close to the superconducting gap value appears in the electronic Raman spectra which is attributed to scattering by paired superconducting quasiparticles. Experimental results from V_3Si ($T_c \sim 17K$) and a theoretical fitting[15] are shown in Fig. 1.3. The peaks near 2Δ are broad and are dependent on the scattering geometry.

For an anisotropic superconducting gap, theoretical calculations [17] predict that the electronic Raman scattering intensity should turn on at the minimum gap value $2\Delta_{min}$ and a broad peak should develop around the maximum gap value $2\Delta_{max}$. If the gap has nodes (zero gap value) at some points of the Fermi surface, the excitation exists everywhere in the low energy region. The calculated result for an anisotropic gap with nodes is shown in Fig. 1.4. Since one can in principle measure the scattering from excitations at

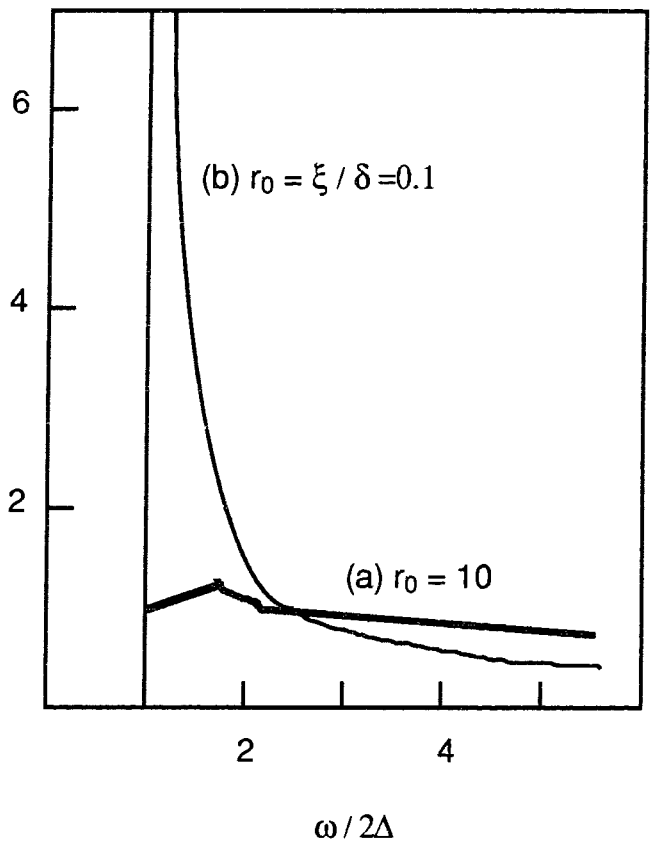

Figure 1.2 Electronic Raman scattering in superconductors in two cases: (a) large wave vector transfer and (b) small wave vector transfer. The horizontal axis is the Raman shift normalized to the energy 2Δ of the superconducting gap and the vertical axis is the scattering intensity in arbitrary units. (Ref. 15)

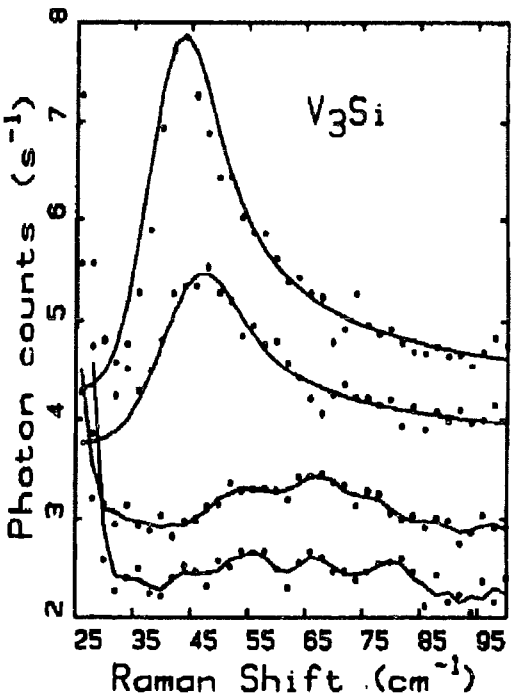

Figure 1.3 Raman scattering from V_3Si. (taken from Ref. 15) Lower two curves are at 40K and upper two are at 1.8K. Symmetries are as follows: top and bottom , 3/4 Eg, middle two, A_{1g} + 1/4 Eg + T_{2g}. Top curve has been shifted upward by 1.0 count/s, middle two curves by 0.5 count/s. Upper two solid curves are theoretical fits, lower two solid curves are three point averages of the data.

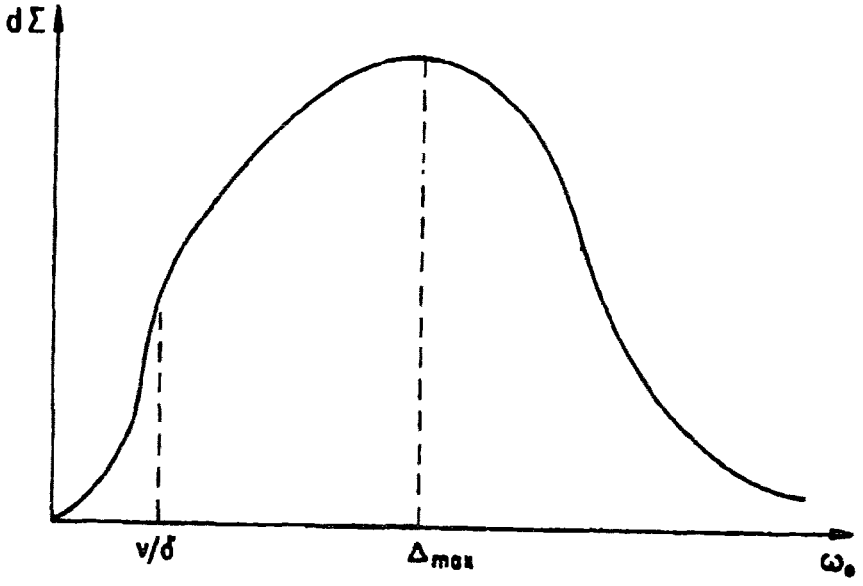

Figure 1.4 Schematic illustration of the Raman spectrum expected as a result of scattering cross a gap with nodes. (Ref. 17)

different parts of the Fermi surface by suitably selecting[15] the polarizations of the incident and scattered light , one has the possibility of measuring any anisotropy in the superconducting gap. This has been demonstrated by Klein and Dierker in spectra obtained from the A15 compounds.[15]

1.2.2 Phonon Raman Scattering from Superconductors

In a conventional superconductor, the superconducting gap is very small. The opening of the gap can only change the distribution of the electronic states in a small region near the Fermi energy. The phonon energies measured in optical experiments are usually much larger than 2Δ and hence the shift of phonon frequencies induced by superconductivity should be very small. However, if a phonon has an energy $\geq 2\Delta$, the phonon's linewidth should broaden when $T< T_c$. The broadening of the linewidth is due to the availability of an additional decay channel for the phonon, namely the breaking up of the paired quasiparticles. For a phonon with an energy far above the gap value, its linewidth should be almost temperature independent when $T < T_c$. For a phonon with an energy much less than the gap value, its linewidth should decrease slightly when $T < T_c$, due to the loss of the decay channel provided by normal electron phonon scattering.

As mentioned above, in conventional superconductors, the gap value is usually smaller than the energy of optical phonons and there are no superconductivity induced effects, commonly called phonon anomalies, for the optical phonons observed in Raman spectra. In conventional superconductors these anomalies have been observed only in neutron scattering studies of

acoustic phonons with energies near the superconducting gap energy.[22,23]

For the high-T_c superconductors, in which the gap energy 2Δ is assumed to be comparable to the optical phonon energies, the superconductivity induced effect on the phonon frequencies and linewidths should become observable in the optical spectra. In the context of BCS theory, in order to account for the high T_c values observed, it is necessary to make the strong coupling assumption. Neglecting the gap anisotropy and the momentum dependence of the electron-phonon coupling constant, R.Zeyher and G.Zwicknagl calculated the superconductivity induced phonon self energy effects for a high-T_c superconductor.[18] They calculated the change of the complex self energy $\Delta\Sigma_\nu = \Delta\omega_\nu - i\,\Delta\gamma_\nu$ due to superconductivity for phonons ν near the center of the Brillouin zone. Here $\Delta\omega_\nu$ is the change in the phonon frequency and $\Delta\gamma_\nu$ is the change in the phonon linewidth (HWHM) for mode ν. Zeyher and Zwicknagl actually carried out these calculations in terms of a polarization Π and their results for the frequency shift can be expressed as [18,19]

$$\Delta\omega_\nu = \frac{\lambda_\nu \omega_\nu}{2} \mathrm{Re}\left(\frac{\Pi}{N(0)}\right) \quad , \qquad 1\text{-}3$$

where λ_ν is the electron phonon coupling constant and N(0) the density of states per spin. The change in HWHM due to superconductivity may be expressed as [18,19]

$$\Delta\gamma_\nu = \frac{\lambda_\nu \omega_\nu}{2} \mathrm{Im}\left(\frac{\Pi}{N(0)}\right) \quad . \qquad 1\text{-}4$$

Zeyher and Zwicknagl have calculated the real and imaginary parts of $\Pi/N(0)$ for various temperatures T below T_c and for different scattering rates which are meant[18] to cover a range extending from a perfectly clean superconductor ($1/\tau 2\Delta = 0$) to a superconductor with many impurities ($1/\tau 2\Delta = 3$). In Fig. 1.5 the superconductivity induced change in $Re(\Pi/N(0))$ for $1/\tau 2\Delta = 0.33$ (a relatively "clean" superconductor) is plotted versus $\omega/2\Delta$ where ω is the phonon frequency and 2Δ is the superconducting gap. In Fig. 1.5, $Re(\Pi/N(0))$ equals zero when the compound is in the normal state and thus the plotted curve represents the change in $Re(\Pi/N(0))$ that one should observe when cooling the sample from T_c to $T = 0.16\ T_c$. In Fig. 1.6, the $Im(\Pi/N(0))$ is shown as a function of $\omega/2\Delta$ again for $T/T_c = 0.16$. In Fig. 1.6, $1/\tau 2\Delta$ is also equal to 0.33. The results may be summarized as follows for such a superconductor:

(1) the phonons near the gap value show the largest frequency softening and linewidth broadening.

(2) phonons below the gap value show some softening which decreases with increasing distance from the gap value.

(3) phonons above the gap value can harden in frequency and broaden in linewidth.

1.3 Far Infrared Experiments in $YBa_2Cu_3O_{7-x}$

In the infrared region, the absorption in high-T_c materials should contain possible contributions from infrared active optical phonons, free carriers, bound carriers and perhaps higher order processes. The free carriers are

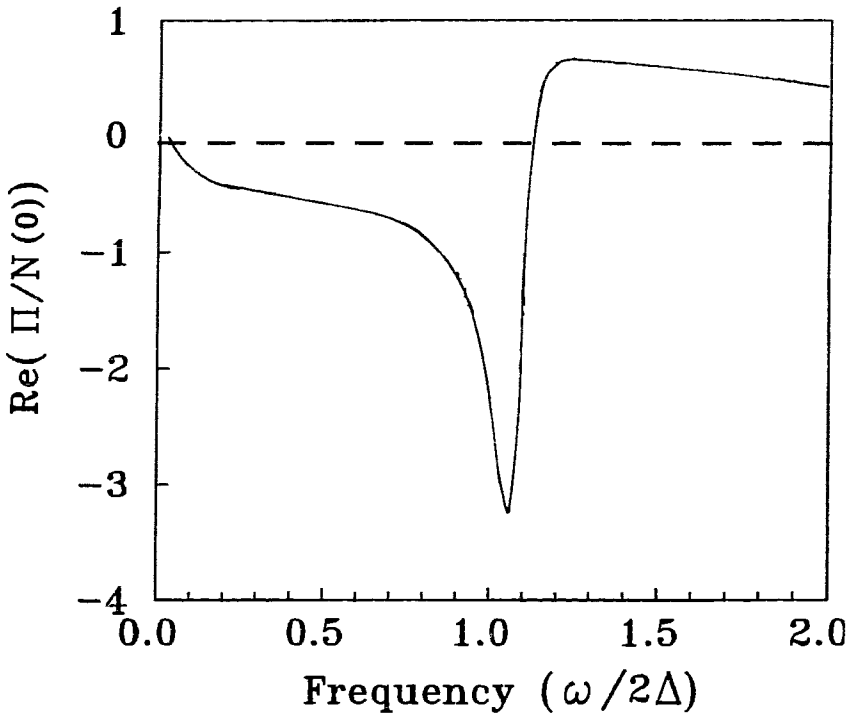

Figure 1.5 Illustration of the superconductivity induced change in the Real part of Π/ N(0) as a function of $\omega/2\Delta$ for $T/T_c = 0.16$ and $1 / \tau 2\Delta = 0.33$. ω is the phonon frequency and 2Δ is the superconducting gap.(Ref. 18)

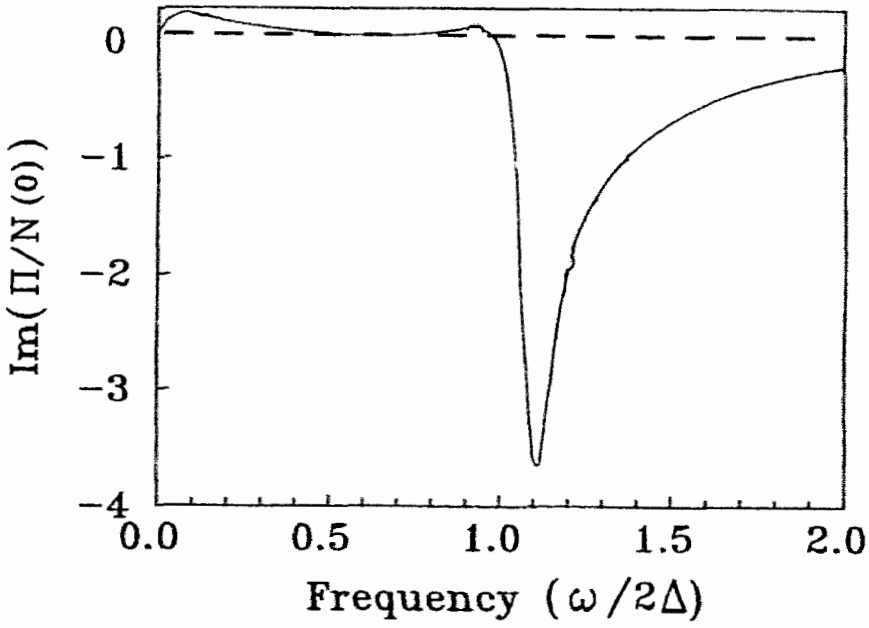

Figure 1.6 Illustration of the superconductivity induced change in the imaginary part of $\Pi/N(0)$ as a function of $\omega/2\Delta$ for $T/Tc = 0.16$ and $1 / \tau 2\Delta = 0.33$. ω is the phonon frequency and 2Δ is the superconducting gap.(Ref. 18)

assumed to be responsible for the dc conductivity and to condense to form the superconducting state at temperatures lower than T_c. In principle, far infrared reflectivity (FIR) experiments should provide a direct probe of the existence and nature of the superconducting gap in these materials. To date, however, FIR spectra in Y123 have not provided any clear evidence of the existence of such a gap. It has been pointed out[20] that this could be due to the fact that Y123 is in the clean limit and hence it would be difficult to observe the gap, because in this case too much of the free carrier spectral weight from the relatively sharp Drude peak is transferred into a δ-function at $\omega = 0$.

FIR spectroscopy also allows one to study the infrared active phonons in high temperature superconductors (HTSC).[21] The interest here stems in part from the possibility that the phonons may contribute to the mechanism of superconductivity. In addition, however, one might expect the HTSC gap to have an energy comparable to that of the optic phonons. In this case, the phonons can exhibit measurable changes in linewidth and frequency (phonon anomalies) as described in the previous section, as the sample is cooled below T_c.

Several FIR experiments[21] have reported superconductivity induced anomalies in the frequencies and linewidths of the infrared c-axis oxygen vibrations in Y123. The anomalies have also been observed in oxygen reduced samples ($x = 0.43$), but in this case the onset temperature of the anomaly was at about 110K which was well above $T_c \sim 60K$.[24] In other words, in oxygen reduced samples the phonon anomalies do not appear to be correlated with the onset of superconductivity. For this reason and others, the phonon

anomaly measurements in Y123 have not led to an accepted value for the superconducting gap. Measurements in $YBa_2Cu_4O_8$ and in Pr and Zn doped samples of the same compound have, however, led to a prediction[21,25] for the gap value in these materials which appears to scale with T_c. Finally, recent FIR measurments of the c-axis conductivity have revealed[26] the possible existence of a pseudo gap such as might occur in a spin fluctuation spectrum.

1.4 Raman Scattering in $YBa_2Cu_3O_{7-x}$

The Raman spectra of $YBa_2Cu_3O_{7-x}$ have unveiled some unusual features which appear to be characteristic of spectra obtained from all the hole doped cuprates.

1.4.1 Electronic Raman Scattering in $YBa_2Cu_3O_{7-x}$

It has been found that in the Raman spectra obtained from all the hole doped cuprate superconductors, there is a strong background scattering or electronic continuum that extends from frequency $\omega \sim 0$ to energy near 1eV in both the normal and superconducting states. It has been shown that the high energy portion ($\omega > 700cm^{-1}$) of these continua appears to be independent of both temperature and oxygen concentration ($0 < x < 0.50$).[27-29] As mentioned previously, if the cuprates represents normal metals, one would expect the normal state continua to be cut off at about $\omega \sim qv_f < 50cm^{-1}$. Thus the fact that the normal state continua in the cuprates extend to energies greater than 1eV represents an as yet unsolved mystery. For our purpose here, however, it is important to note that the intensities of both the A_{1g} and B_{1g}

continua in Y123 have been found to be independent of energy (that is the A_{1g} and B_{1g} continua are essentially flat for Raman shift larger than 700cm^{-1}), oxygen concentration x and temperature T. Fig. 1.7 shows two typical electronic Raman spectra from $YBa_2Cu_3O_{7-x}$ after subtraction [30] of the phonons from the original spectra.

In Fig. 1.7, it can be seen that the peak positions of the low energy part of electronic continua are dependent on the scattering geometry. This reminds us of the electronic scattering by superconducting carriers in A-15 compound.[14-16]

Finally it should be noted that spectra similar to those shown in Fig. 1.7 have been observed for both the Bi and Tl - based compouds.[31,32] It has been pointed out[31] that these spectra must arise from excitations in the CuO_2 planes, which are the only common element of all these compounds.

1.4.2 Phonon Raman Scattering in $YBa_2Cu_3O_{7-x}$

The phonon Raman spectrum of Y123 will be discussed in detail in chapter 3. In general such spectra contain five phonon peaks. In the context of the tetragonal point group four of these have A_{1g} symmetry and one at 340cm^{-1} has B_{1g} symmetry. The latter phonon has been observed in some samples to undergo dramatic changes in frequency and linewidth[11,12,33-35] when cooled below T_c. The A_{1g} phonons exhibit less dramatic anomalies in frequency and linewidth.[34-36] Thus the B_{1g} phonon behavior has attracted the most attention and we will briefly review some results. In a sample with x = 0.00, the linewidth of the B_{1g} phonon abruptly broadens by 8cm^{-1} and the

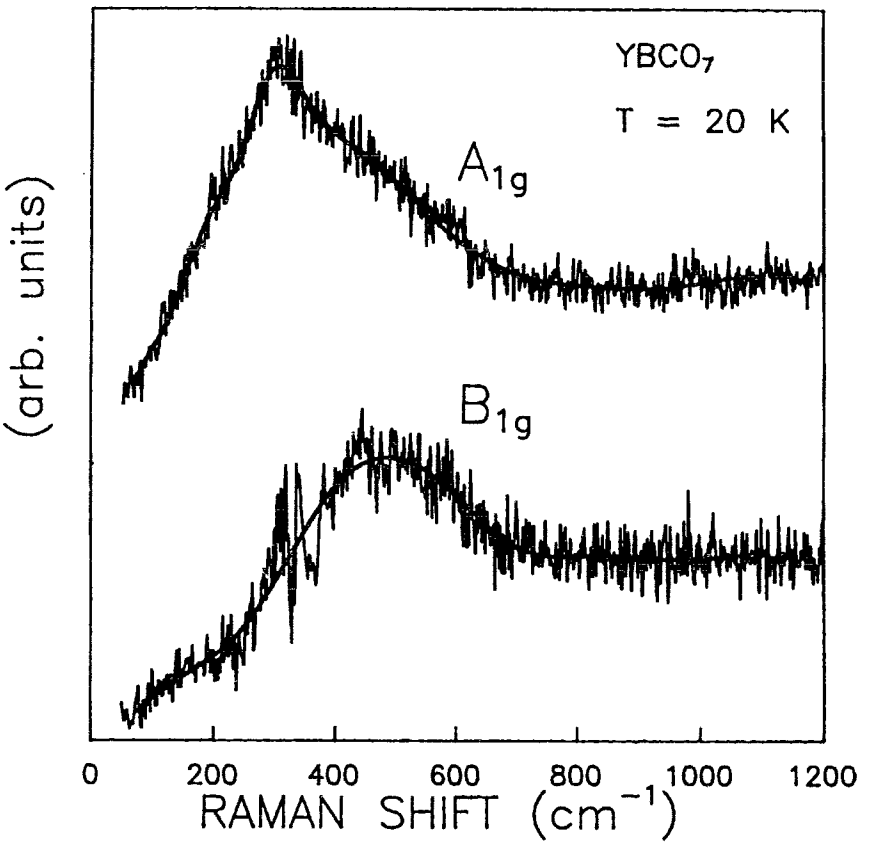

Figure 1.7 Electronic Raman scattering from $YBa_2Cu_3O_7$ at 20K. in different scattering configurations. The A_{1g} spectrum has been shifted upward relative the B_{1g} spectrum (Ref.30).

frequency softens by $8cm^{-1}$ when the sample is cooled below T_c.[35] For x = 0.07, the linewidth of the same phonon exhibits a small broadening and the softening of the frequency is reduced to about $4cm^{-1}$.[35]

From the strong coupling theory developed by R. Zeyher and G. Zwicknagl as described in **1.3.2**,[18] the energy and linewidth of the B_{1g} phonon should provide an estimate of the superconducting gap. If a single sharp gap is assumed, then from comparison between theory and experimental results, it has been found that for x = 0.00(T_c = 89.7K), the results yield a value for the superconducting gap of about $340cm^{-1}$; for x = 0.07(T_c =93.7K), about $400cm^{-1}$. [35] It seems that the superconducting gap determined in this manner is very sensitive to doping level. This result must be viewed with some suspicion since it is difficult to explain how the superconducting gap can change by 20% while T_c changes by only 4%. Also since doping is expected[37] to induce only small changes in the Fermi surface associated with the CuO_2 planes, the sensitivity of the B_{1g} phonon anomaly and the behavior of the peak feature in the B_{1g} continuum to the doping level cannot be explained by the changes of the Fermi surface.

Finally it should be noted that in contrast to the sensitivity of the B_{1g} phonon anomaly to doping, the magnitude of the phonon anomalies exhibited by the A_{1g} phonons are essentially constant throughout the range x = 0.00 to x = 0.07.[35]

In recent experiments it has been found that the A_{1g} continuum remains virtually unchanged as x is varied from 0.00 to 0.07.[30] The B_{1g} continuum, however , changes dramatically in this same region with the major feature

being a shift in the distribution (by about $80cm^{-1}$) to higher energies as x is increased from 0.00 to 0.07.[30] These experiments established a strong correlation between the doping dependence of the B_{1g} phonon anomaly and the B_{1g} electronic continuum (and the A_{1g} phonon anomalies and the A_{1g} electronic continuum). It was thus demonstrated that the B_{1g} phonon interacts with the B_{1g} continuum and the A_{1g} phonons with the A_{1g} continuum. This dichotomy had not been incorporated into previous interpretations of the phonon anomaly experiments and now raised the possibility of an anisotropic gap or the existence of multiple gaps. In a recent paper[38] , the Raman spectrum was calculated by using a tight binding model to determine the Fermi surface and assuming the existence of a d-wave gap in Y123. This calculation produced a good fit to the low energy A_{1g} continuum ($T < T_c$), but the calculated B_{1g} continuum was weaker and lower in energy than the measured value. This has raised questions concerning the origin of the B_{1g} continuum which will be discussed in more detail in section 4.6.4.

1.4.3 The Phonon Intensity Anomalies in $YBa_2Cu_3O_{7-x}$

The intensities of the phonons in Y123 have been measured as a function of temperature by different groups.[38-41] In general it is found that the phonon intensities increase markedly as the sample is cooled below T_c. One might expect such an enhancement if the phonon energy is close to the gap energy and hence it could experience a resonant enhancement on cooling below T_c. To date, the most detailed measurements have been carried out by the Stuttgart group.[41] Their experiments were carried out on a predominantly c-

axis oriented film of $YBa_2Cu_3O_7$ and their results were interpreted in terms of a single sharp superconducting gap. Their main results were:

(1) The observed effects were essentially independent of laser excitation energy.

(2) The superconductivity induced intensity anomalies were attributed to a resonant Raman process involving phonon coupling across the gap.

(3) Intensity changes in the normal state did not follow the expected Bose-Einstein factor dependence and were attributed to resonance of the phonons with temperature dependent excitation energies across the Fermi surface (two CuO_2 plane bands must cross the Fermi level).

In this thesis, we will focus our attention on the superconductivity induced intensity anomalies($T \leq T_c$) and report the results of Raman scattering experiments carried out on single crystals of $YBa_2Cu_3O_{7-x}$ with oxygen concentration in the range $0.00 \leq x \leq 0.07$. The primary purpose of these experiments is to examine the doping dependence of the observed superconductivity induced anomalies. Assuming the anomaly arises because of resonance between the phonons and a gap,[41] this should provide indirect information on the doping dependence of the gap. The results should of course be consistent with the doping dependence of 2Δ as determined from phonon anomaly experiments[11,12,35] and with the results obtained from direct measurements of the electronic continua.[30,33,34] Thus the intent is to determine first if the intensity anomaly results are consistent with the picture obtained from previous experiments. In so doing we will also be testing the applicability of the resonance mechanism proposed[41] by the Stuttgart group. In this regard,

since the B_{1g} phonon couples to the B_{1g} continuum and the A_{1g} phonons to the continuum of the same symmetry[30] and the gaps in these continua are quiet different, the assumption of the resonance between the phonons and gaps must be reviewed in this context.

Our results show a superconductivity induced enhancement of the B_{1g} phonon intensity which decreases as x is increased. The sensitivity of the enhancement in the B_{1g} phonon intensity to the doping level is consistent with the doping dependence of the B_{1g} continuum[30] and the B_{1g} phonon anomaly.[35] A rough estimate for 2Δ has been obtained from these intensity measurements and this estimate is in reasonable agreement with values determined from B_{1g} phonon anomaly measurements.[35] For the $115cm^{-1}$ A_{1g} phonon, the intensity enhancements are almost independent of oxygen concentration. This is consistent with the observed behavior of the A_{1g} continuum.[30] The results for $115cm^{-1}$ phonon indicate resonance with excitations having energy lower than the accepted gap value of $2\Delta \approx 300cm^{-1}$ and thus might be consistent with the existence of a d-wave gap. These results and those for the remaining A_{1g} phonons will be discussed in detail in Chapter 4 of this thesis. Chapter 2 will provide a brief review of the Raman scattering process and Chapter 3 will give a detailed review of the Raman scattering results obtained to date from Y123. Chapter 5 will describe our conclusions and suggestions for further work.

Chapter 2
Light Scattering by Phonons

The inelastic light scattering by optical phonons is often called Raman scattering by phonons. If the frequency of the incident light is ω_L, the frequency of the scattered light ω_S will be shifted by a phonon frequency ω_P relative to ω_L.

2.1 The Phenomenological Theory of Raman Scattering[42]

When a beam of polarized light is incident on a piece of material, it will induce a polarization in the material. The induced polarization P can be expressed as

$$P = \alpha E_0 \cos\omega_L t,$$

where α is the polarizability of the material, E_0 the amplitude of the electric field of the incident light and ω_L the frequency of the incident electric field. The vibrations of the lattice will modulate the polarizability. We can expand the polarizability near the thermal equilibrium positions of the lattice,

$$\alpha = \alpha_0 + \Sigma(\frac{\delta\alpha}{\delta Q_\alpha})_0 Q_\alpha + \ldots\ldots , \qquad 2\text{-}1$$

where α_0 is the rigid lattice polarizability and 0 indicates the thermal equilibrium positions of the lattice. $Q_\alpha = Q_\alpha^0 e^{i(\mathbf{q}\cdot\mathbf{r}-\omega qt)}$ is one of the normal coordinates of the normal modes of the lattice vibrations. $\mathbf{q}$ and ω_q are the wave vector and the frequency respectively of the lattice vibration . The sum is taken over all the normal coordinates of the lattice vibrations. For simplicity, we only consider the contribution from one normal coordinate here.

For small amplitudes and the long wavelength (see the next section), we can take 2-1 to its first order and rewrite the polarizability as

$$\alpha = \alpha_0 + \alpha_1 \cos\omega_P t \ ,$$

where α_1 is a constant. Substituting α into the expression for the induced polarizability P, we will have

$$P = \alpha_0 E_0 \cos\omega_L t + \frac{1}{2}\alpha_1 E_0[\ \cos(\omega_L-\omega_q)t + \cos(\omega_L+\omega_q)t\ ]. \qquad 2\text{-}2$$

The induced polarization P contains three terms. Since the scattered light can be considered as the radiation field of the induced polarization, the spectrum will contain components at three different frequencies. One of these occurring at the laser frequency is the first term in 2-2, which is the elastic Rayleigh scattering. The second occurs at $\omega_L-\omega_q$ and is called the Stokes scattering and the third at $\omega_L+\omega_q$ is the anti-Stokes scattering.

If the material is anisotropic, the polarizability will be a second rank tensor. An arbitrary component of the polarizability tensor can be written as

$$\alpha_{ij}=\alpha^0{}_{ij}+\left(\frac{\delta\alpha_{ij}}{\delta Q_\alpha}\right)_0 Q_\alpha + \ldots\ldots \qquad 2\text{-}3$$

Since the components of a second rank tensor transform as the products (x^2, y^2, z^2, xy, yz and xz)of the orthogonal Cartesian coordinates under the operations of the symmetry group of the material, according to 2-1, the Raman active normal modes (Q_α) of the lattice vibrations should also transform as the products of the orthogonal Cartesian coordinates.

2.2 The Selection Rules

In the quantum theory of lattice vibration, the vibrational energy of each normal mode is quantized into units called phonons characterized by their frequency ω_p. In the Rayleigh scattering, no phonons are absorbed or emitted. In the Stokes scattering, one or more phonons are emitted; the frequency of the scattered light is $\omega_S = \omega_L - n\omega_p$. n is an integer. In the anti-Stokes scattering, one or more phonons are absorbed, $\omega_S = \omega_L + n\omega_p$.

In any first order Raman scattering process, the conservation of energy and momentum must be satisfied. If we only consider one phonon processes,

$$\omega_L = \omega_S + \omega_p \quad \text{and} \qquad 2\text{-}4$$

$$\mathbf{q_L} = \mathbf{q_S} + \mathbf{q_p} \qquad 2\text{-}5$$

where $\mathbf{q}$ is the wave vector of the photon ($\mathbf{q_L}$,$\mathbf{q_S}$) or phonon ($\mathbf{q_p}$). For the photons in the frequency region of the visible light, the photon's wave number is very small when compared with the dimension of the first Brillouin zone of the material. As a result, it is usually said that the scattering is from q=0 phonons. The vibrations with q=0 are invariant under some of the symmetry operations of the point group of the material. The point group of the material can always be decomposed into several irreducible representations. Among the irreducible representations of the point group, some have the products of the orthogonal Cartesian coordinates as their basis functions. The Raman active phonons should transform like these irreducible representations as mentioned above. On the other hand, any product of the orthogonal Cartesian coordinates is invariant about the inversion center of the material. In any material where there is an inversion center, all the Raman active phonons will transform as the even representations.

As shown by the phenomenological theory, the scattered light can be taken as the radiation field of the induced dipole moment. For dipole radiation, the radiated electric field is proportional to $(\mathbf{r}_0 x \mathbf{p}) x \mathbf{r}_0$, where $\mathbf{p}$ is the electric dipole moment and $\mathbf{r}_0$ is the unit vector between the position of the scattering source and the position where the scattered (radiated) electric field is measured. For a particular polarization $\mathbf{E_S}$, where $|\mathbf{E_S}|$ is the amplitude of the scattered field, the scattered light intensity is given by

$$| \mathbf{E_S} \cdot (\mathbf{r}_o x \mathbf{p}) x \mathbf{r}_o)|^2 \sim |\mathbf{E_S} \cdot \alpha \cdot \mathbf{E_L}.|^2 , \qquad 2\text{-}6$$

where α is the polarization tensor, $\mathbf{P} \sim \alpha \mathbf{E_L}$ and $|\mathbf{E_L}|$ is the amplitude of the incident field.[43] Only when $\varepsilon_S \cdot \alpha \cdot \varepsilon_L$ is non zero, where ε_S and ε_L are the unit vectors of the polarizations of the incident and the scattered light, the scattering intensity is non zero.

For the lattice associated with a given structure, the polarizability tensors have been tabulated for each irreducible representation that transform as the products of the orthogonal Cartesian coordinates. Using 2-6, we can find the scattering geometries (the orientations of the polarizations of the incident and the scattered light) which will lead to the maximum scattering intensity. The selection of appropriate geometric configurations thus enables us to satisfy the selection rules.

2.3 The Microscopic Theory of Raman Scattering by Phonons[44]

A physical picture of a Raman scattering process is shown in Fig 2.1. A Raman scattering process can be described by three consecutive steps. First, the incident photon with frequency ω_L interacts with an electronic state, for

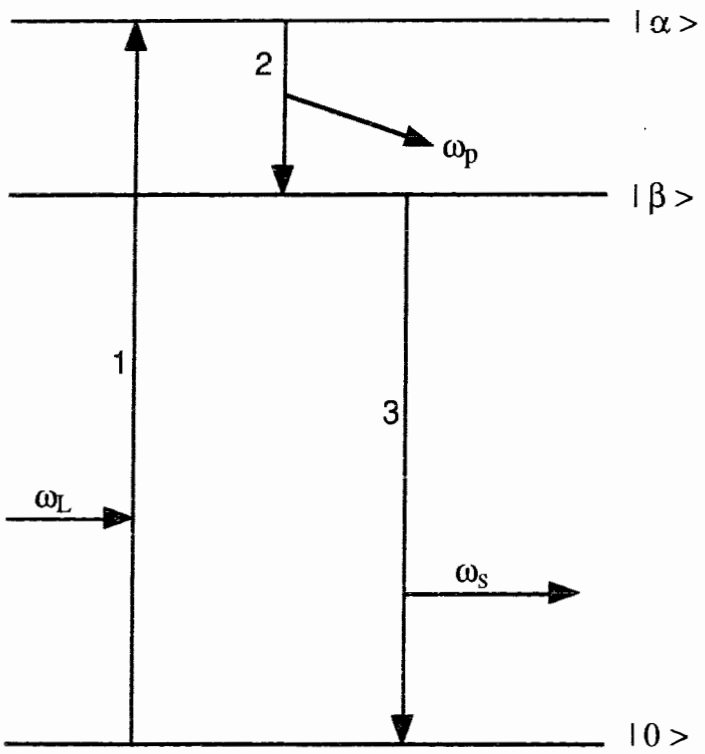

Figure 2.1 One of the time sequences in Stokes Raman Scattering.

example the ground state $|0\rangle$: an electron is excited to a higher energy level $|\alpha\rangle$. Second, the electron in the excited state $|\alpha\rangle$ relaxes to another excited state $|\beta\rangle$ with the emission of a phonon of frequency ω_p. Third, the electron in state $|\beta\rangle$ recombines with the hole created in the $|0\rangle$ state and then emits a photon with frequency ω_S. When $\omega_S<\omega_L$, the scattering process is called Stokes scattering; when $\omega_S>\omega_L$, anti-Stokes scattering. Since the three steps involved could happen in any time sequence, there are always six possible time sequences for each Raman scattering process. The scattering cross-section can be given by the third order perturbation theory.

The ratio of the probability of a Stoke scattering process to that of an anti-Stokes scattering process is approximately $\exp(\omega_p/k_bT)$ when $\omega_p << \omega_L$ and ω_S, and where k_b is the Boltzman constant. Since at low temperatures, the probability for the anti-Stokes scattering is very small, we will only consider the Stokes scattering from now on.

The initial state of the system consisting of material , incident and scattered light can be expressed as

$$|i\rangle = |0\rangle|p\rangle|n_L,n_S\rangle ,$$

where $|0\rangle$ is the ground state of the electrons, $|p\rangle$ one of the excited states of the phonons and $|n_L,n_S\rangle$ the state of the incident and scattered photons characterized by the numbers of the photons. The final state of the system is

$$|f\rangle = |0\rangle|p+1\rangle|n_L-1,n_S+1\rangle.$$

The intermediate states for Fig. 2.1 could be

$$|k\rangle = |\alpha\rangle|p\rangle|n_L-1,n_S\rangle \text{ and}$$

$$|k'\rangle = |\beta\rangle|p+1\rangle|n_L-1,n_S\rangle .$$

The scattering can be described by the matrix element

$$\langle f| H |i\rangle = \langle f| H_1 |k'\rangle\langle k'| H_{eL}|k\rangle\langle k| H_1 |i\rangle,$$

where H is the full Hamiltonian of the system, H_1 the Hamiltonian for the interactions between light and the electrons and H_{eL} the Hamiltonian for the interactions between electrons and phonons. The scattering probability given by the third order perturbation theory is

$$W=\text{const.}\left|\sum_{k',k} \frac{\langle f| H_1| k'\rangle \langle k'| H_{eL}|k\rangle \langle k| H_1| i\rangle}{\omega_{k'i}\omega_{ki}}\right|^2 (1 + n(\omega)), \qquad 2\text{-}7$$

where $n(\omega)$ is the Bose-Einstein factor, the denominators are

$$\omega_{ki} = E_\alpha/\hbar - \omega_L \quad \text{and} \qquad 2\text{-}8$$

$$\omega_{k'i} = E_\beta/\hbar + \omega_p - \omega_L . \qquad 2\text{-}9$$

Here we have already expressed the energies of the electronic states as $E_\alpha = \hbar\omega_\alpha$ and $E_\beta = \hbar\omega_\beta$. Both the states $|\alpha\rangle$ and $|\beta\rangle$ are virtual states.

Considering $H_1 = -\frac{e}{m}(\mathbf{p}\cdot\mathbf{A})$, where e is the charge of an electron, m the mass, **p** the momentum and **A** the vector potential , we can rewrite 2-7 in this way

$$W \sim \left|\frac{(\boldsymbol{\varepsilon}_L\cdot\mathbf{p}_{\alpha\theta})\,(\boldsymbol{\varepsilon}_s\cdot\mathbf{p}_{\theta\beta})\,\langle k'|H_{eL}|k\rangle}{(\omega_\beta+\omega_p-\omega_L)\,(\omega_\alpha-\omega_L)}\right|^2 (1 + n(\omega)) . \qquad 2\text{-}10$$

We call $\frac{\mathbf{p}_{\alpha\theta}\mathbf{p}_{\theta\beta}\,\langle k'|H_{eL}|k\rangle}{(\omega_\beta+\omega_p-\omega_L)\,(\omega_\alpha-\omega_L)}$ the Raman tensor **R** . Of course, **R** is proportional to the polarizability tensor α . It is worth to remember that 2-10

only corresponds to the time sequence in Fig. 2.1

When $|\alpha>$ is a real state, the intensity which is proportional to the transition probability will resonate with ω_L. The intensity will be proportional to

$$\frac{1}{(\omega_\alpha-\omega_L)^2} \qquad 2\text{-}11$$

Since there are six possible time sequences, the denominators in 2-7 are different for different time sequences.

In this thesis, we are interested in the process in which there is a resonance between the phonon energy and a gap. Let us consider the following process which is shown schematically in Fig. 2.2 . The ground state for holes is just above an energy gap, one of the intermediate state is well below the bottom of the gap and the other is just below the bottom of the gap. First, a hole is created in $|\alpha>$ with the absorption of an incident photon ω_L. Second the hole in $|\alpha>$ relaxes to $|\beta>$ with the emission of a Stokes photon ω_S. Third, the hole at $|\beta>$ recombines with the electron at the top of the gap and then emits a phonon ω_p.

For this process, $|i> = |0>|p>|n_L,n_S>$,

$|k> = |\alpha>|p>|n_L-1,n_S>$,

$|k'> = |\beta>|p>|n_L-1,n_S+1>$ and

$|f> = |0>|p+1>|n_L-1,ns+1>$.

The denominators entering into the scattering probability are

$$\omega_{ki} = E_\alpha/\hbar - \omega_L \quad \text{and} \qquad 2\text{-}12$$

$$\omega_{k'i} = E_\beta/\hbar - \omega_L + \omega_S = E_\beta/\hbar - \omega_p \; . \qquad 2\text{-}13$$

We can also express $\omega_{k'i}$ in another way

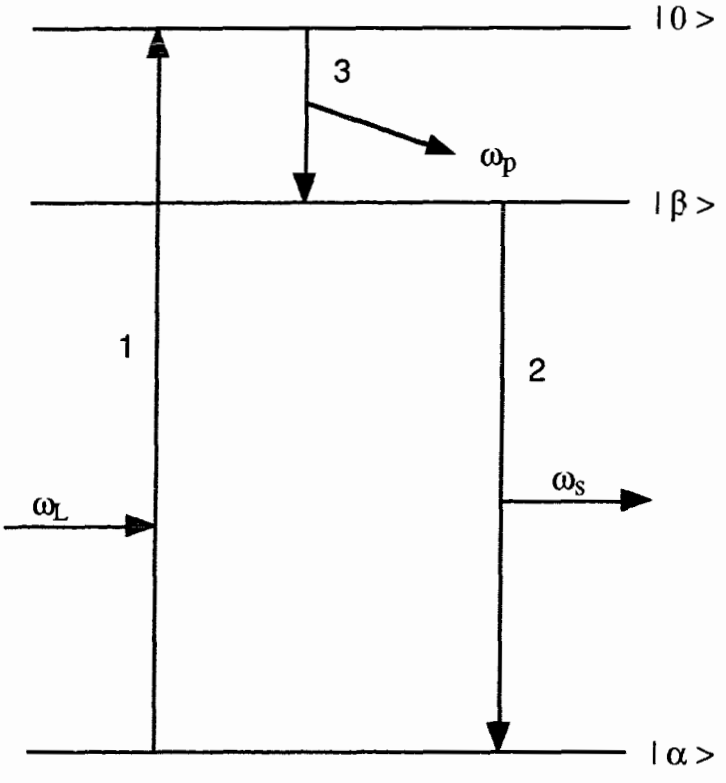

Figure 2.2 Anothe time sequence in Stokes scattering.

$$\omega_{k'i} = \text{the gap width}(\ \omega_g\ ) - \omega_p.$$

When the phonon energy is close to the gap width, we expect a strong resonance between the gap width and the phonon energy. If $|\alpha>$ is only a virtual state, the intensity of the scattered light will be proportional to

$$\frac{1}{(\omega_g-\omega_p)^2} \qquad 2\text{-}14$$

2.4 The Phonon Intensities

If we measure the phonon intensity by the number of collected photons with $\omega_S = \omega_L - \omega_p$, the intensities of the scattered light and the phonon are equal. This is just the case for Raman spectra. The line shape of the scattered light is determined by the decay process of the corresponding phonon and the attributes of the spectrometer system.

2.4.1 The Lorentzian Profile

In the vibrational Raman spectra obtained from most solids at low temperatures (< 300K) the phonons are homogeneously broadened and the lineshapes are well described by a Lorentzian profile

$$I_L=\frac{A_1}{(\omega-\omega_p)^2+\gamma^2} \quad , \qquad 2\text{-}15$$

where A_1 is a constant, ω_p the phonon's frequency and γ the half width at half maximum which is related to the lifetime of the phonon.

A Lorentzian profile is symmetric about ω_p. The integrated intensity of the phonon is

$$\int_{-\infty}^{\infty} \frac{A_1}{(\omega-\omega_p)^2+\gamma^2} d\omega = \pi \frac{A_1}{\gamma} \qquad 2\text{-}16$$

2.4.2 The Fano profile

Suppose a phonon couples with a smooth electronic continuum, as shown in Fig. 2.3. In Fig. 2.3, the unperturbed system has a ground state $|g\rangle$, an electronic continuum characterized by the density of the states $\rho(E)$ and an excited phonon state $|p\rangle$ with energy E_p. The continuum and $|p\rangle$ couple through a matrix element V. Transitions to the continuum and the excited phonon state are Raman active and with Raman matrix element T_e and T_p respectively. For simplicity, we take V, T_e and T_p as real and constant. Klein has shown that the scattered intensity is given by[13]

$$I_F = \frac{\pi\rho(E)T_e^2(E_p - E - \frac{VT_p}{T_e})^2}{(E_p - E + V^2R(E))^2 + \pi^2V^4\rho(E)} . \qquad 2\text{-}17$$

In 2-18, R(E) is the real part of the electronic response function. Define

$$\Gamma = \pi V^2\rho(E) \qquad 2\text{-}18$$

as the broadenigh due to the interactions (half linewidth at half maximum, HWHM), then further define

$$\varepsilon = \frac{E - E_p - V^2R(E)}{\pi V^2\rho(E)} \quad \text{and}$$

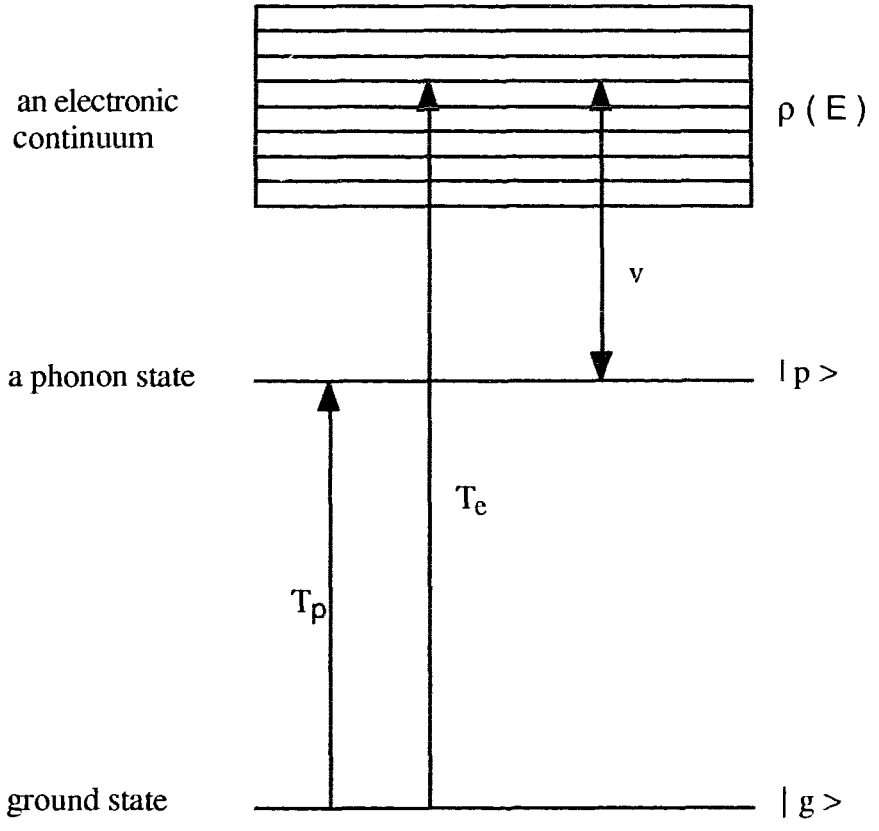

Figure 2.3 A smooth electronic continuum couples with a phonon state.

$$q = \frac{\frac{T_p V}{T_e} + V^2 R(E)}{\pi V^2 \rho(E)} . \qquad 2\text{-}19$$

Using these definitions, we can rewrite 2-18 as

$$I_F = \pi \rho(E) T_e^2 \frac{(\varepsilon + q)2}{1 + \varepsilon^2} . \qquad 2\text{-}20$$

In a small region near the phonon energy, the continuum should be smooth and we can take $\rho(E)$=const. as an approximation and from 2-19 we also have a constant Γ in this same frequency range.

Finally, we have

$$I_F = A_{2^*} \frac{(\varepsilon+q)^2}{1+\varepsilon^2} , \qquad 2\text{-}21$$

where A_2 is a constant. Equation 2-22 is usually called a Fano profile.

In the strongly interacting case, a Fano profile is very asymmetric. The asymmetric property of a Fano profile is characterized by q, the asymmetry parameter. The extrema of the intensity happens at $\omega_p \pm \gamma/q$. The minimum intensity is zero. The smaller the absolute value of q, the more asymmetric the Fano profile becomes. When $q < 0$, as ω deviates gradually from ω_{max} where the intensity reaches its maximum, the intensity of the low frequency side decreases slower than the high frequency side does. When $q > 0$, it is the high frequency side where the intensity decreases slower than that of the low frequency side. When q approaches infinity, a Fano profile approaches a Lorentzian profile. The calculated Fano line shape for various q[19] is shown in Fig. 2.4.

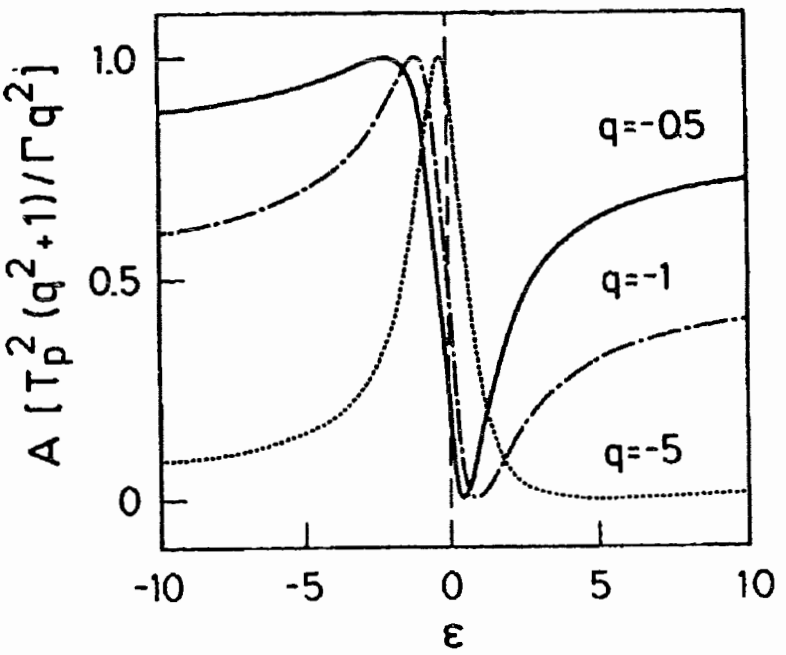

Figure 2.4 Fano line shapes for different asymmetric parameter q.

(taken from Ref. 19)

The integrated intensity of the Fano profile can be expanded to reflect various contributions

$$\int_{-\infty}^{\infty} A_2 \frac{(\varepsilon+q)^2}{1+\varepsilon^2}\, d\omega = \int_{-\infty}^{\infty} \frac{A_2 q^2}{1+\varepsilon^2}\, d\omega + \int_{-\infty}^{\infty} \frac{2A_2 \varepsilon q}{1+\varepsilon^2}\, d\omega + \int_{-\infty}^{\infty} \frac{A_2 \varepsilon^2}{1+\varepsilon^2} d\omega \quad . \quad 2\text{-}22$$

There are three terms in the expansion. The first term is basically from the phonon contribution. The second term is from the interaction between the phonon and the continuum. The third term involves only the continuum. The integrated phonon intensity in a Fano profile is

$$\int_{-\infty}^{\infty} I_F(\omega) d\omega = \pi A_2 q^2 \gamma. \qquad 2\text{-}23$$

Chapter 3
Raman scattering in $YBa_2Cu_3O_{7-x}$

3.1 The Raman Active Phonons in $YBa_2Cu_3O_{7-x}$[45,46]

3.1.1 Group Theory Predictions about The Raman Active Phonons in $YBa_2Cu_3O_{7-x}$

The parent compound of $YBa_2Cu_3O_{7-x}$ (Y123) is the antiferromagnetic insulator $YBa_2Cu_3O_6$ whose unit cell is tetragonal as shown schematically in Fig. 3.1 . Upon doping with oxygen, the long range antiferromagnetic correlation is gradually destroyed and for higher oxygen concentration, $x \leq 0.6$, the material becomes metallic and superconducting at low temperatures. The unit cell of metallic Y123 is orthorhombic as shown schematically in Fig. 3.2. The Y atom is at the inversion center of the unit cell.

The uint cell is defined such that **a** is parallel to the x-axis, **b** to the y axis and **c** the z-axis. The structural differences between the tetragonal $YBa_2Cu_3O_6$ and orthorhombic $YBa_2Cu_3O_7$ are mainly in the Cu(1)-O(1) planes parallel to the a-b planes. In the tetragonal $YBa_2Cu_3O_6$, there are no bridging O atoms (O(1) atoms) in the y direction.

The symmetry of the unit cell of metallic Y123 can be described by the point group D_{2h}. The sites occupied by Cu(1), O(1) and Y atoms have the full symmetry of the point group while the sites occupied by O(4), Ba, Cu(2), O(2) and O(3) atoms have a lower symmetry C_{2v}. The symmetry of the normal modes of atomic vibrations can be characterized by the symmetry of the corresponding sites. The normal modes must transform like one of the irreducible representations of the symmetry group to which the sites belong.

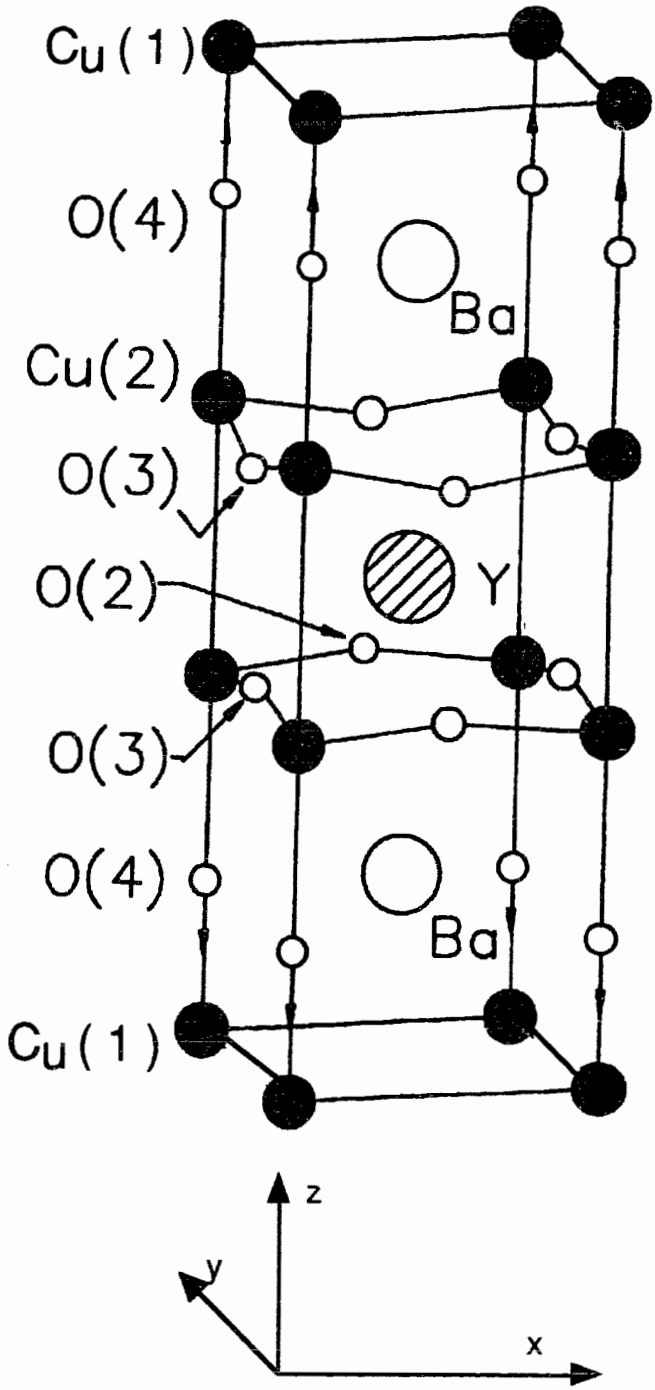

Figure 3.1 a unit cell of $YBa_2Cu_3O_6$

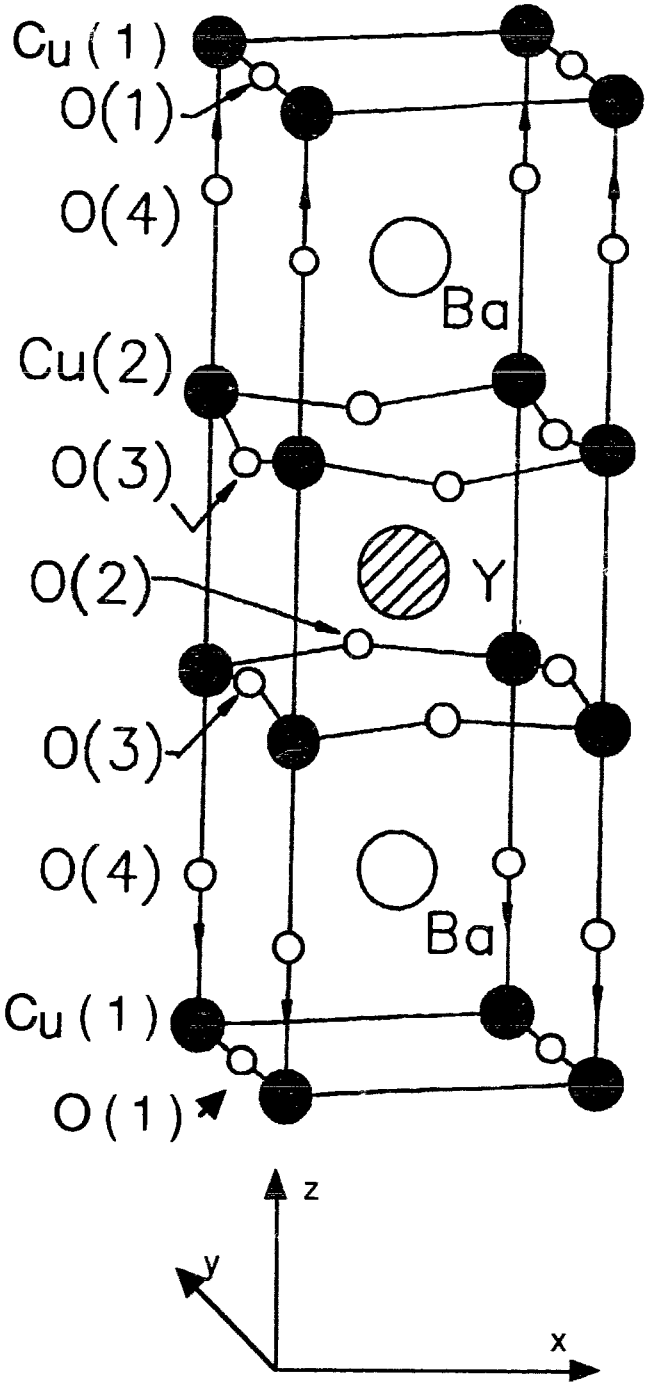

Figure 3.2 a unit cell of $YBa_2Cu_3O_7$

The irreducible representations of the normal modes associated with the D_{2h} sites are B_{1u} , B_{2u} and B_{3u}, where u indicates the representations are odd. Therefore the normal mode vibrations involving Cu(1), O(1) and Y atoms are not Raman active. The irreducible representations of the normal modes for the C_{2v} sites are A_g, B_{1u}, B_{2g}, B_{2u}, B_{3g} and B_{3u}, where g indicates the corresponding representations are even. There are in total 15 optical modes (5 A_g + 5 B_{2g} + 5 B_{3g}) which are Raman active.[45]

Group theory analysis can only determine the symmetry properties of the Raman active modes. The lattice dynamic calculations have to be performed in order to find the eigenenergies and eigenvectors of those modes. The simplest method is the normal mode method. In the normal mode method, the atoms and the interatomic bonds are modeled by point masses and Hookean springs respectively. The equations of motion for the atoms are written in the harmonic approximation and the spring constants associated with each bond are determined by the experiment data.[47] The shell model that has been used in the calculation for high-T_c superconductors takes both the short range forces derived from a Born-Mayer potential and the long range Coulomb forces into consideration. The parameters needed were taken from compounds which are well known and similar to the material studied and refined for a stable lattice. The calculation by W.Kress et al[48,49] made good predictions for the phonons in $YBa_2Cu_3O_7$. The eigenenergies and eigenvectors of the phonons can also be determined from the calculation of the band structure by local density approximation. The full potential function and the dynamic matrix are involved.[50]

3.1.2 Raman Active Phonons Observed Experimentally in $YBa_2Cu_3O_{7-x}$

Experimentally, the five A_g modes are the only Raman active phonons that are normally observed in spectra obtained from Y123[45]. The modes with Ag symmetry have the full symmetry of the D_{2h} point group and the vibrations involved are all in the z-direction. They are the vibrations of the Ba atoms at 115cm^{-1}, the vibration of the Cu(2) atoms at 150cm^{-1}, the out-of-phase vibration of the O(2)and O(3) atoms at 340cm^{-1} , the in-phase vibrations of the O(2) and O(3) atoms at 440cm^{-1} and the vibration of the O(4) atoms at 500cm^{-1} as shown in Fig. 3.3. Fig. 3.4 shows a spectrum from a polycrystalline Y123 sample. If one has a good quality single crystal , it is also possible (but more difficult) to observe the B_{2g} and B_{3g} phonons.[51] These B_{2g} and B_{3g} "pairs" occur at 70 and 83cm^{-1}, 142 and 140cm^{-1}, 210 and 303cm^{-1}, and 579 and 526cm^{-1}.[51] The atomic displacements associated with the B_{2g} and B_{3g} modes are in the x- and y-directions respectively. The assignment of the B_{2g} and B_{3g} modes are only possible by studying untwinned samples. In $YBa_2Cu_3O_6$, which belongs to the D_{4h} point group, the out-of-phase vibration of O(2) and O(3) atoms has B_{1g} symmetry. The B_{1g} symmetry only contains one two fold rotation axis parallel to the z-axis. The two fold rotation axis is retained in $YBa_2Cu_3O_7$, in which there are only two fold rotation axes. The vibrations associated with all the other A_g phonons in D_{2h} have the A_{1g} symmetry in D_{4h}, the full symmetry of the D_{4h} point group. People usually refer all these modes to the representations of D_{4h} because of the small deviation of the orthorhombic $YBa_2Cu_3O_7$ from the tetragonal $YBa_2Cu_3O_6$.

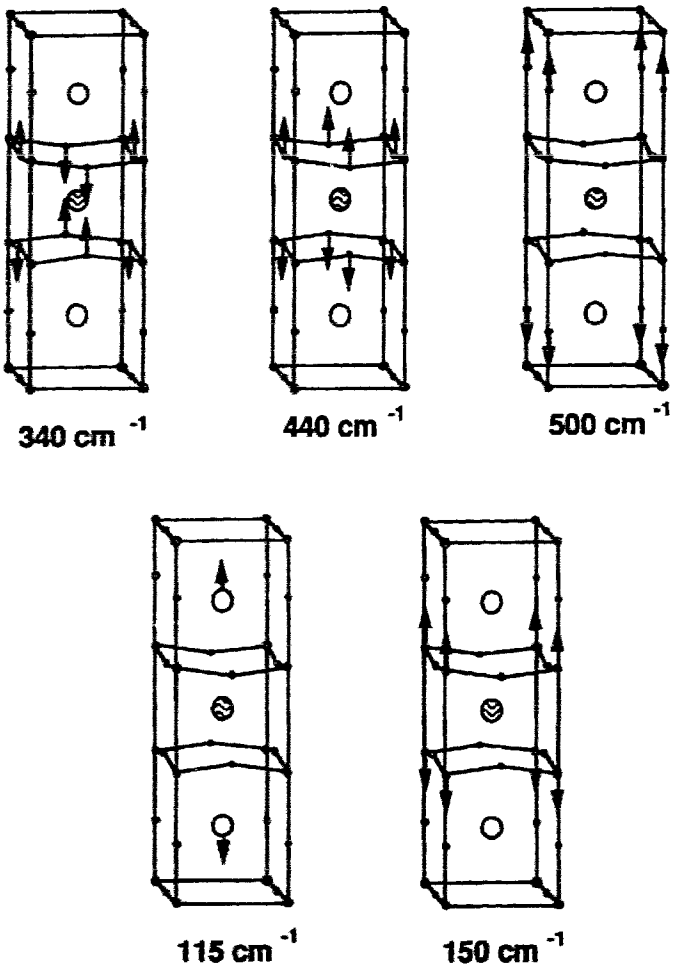

Figure 3.3 The atomic displacement patterns associated with the five Ag modes. (Ref. 43)

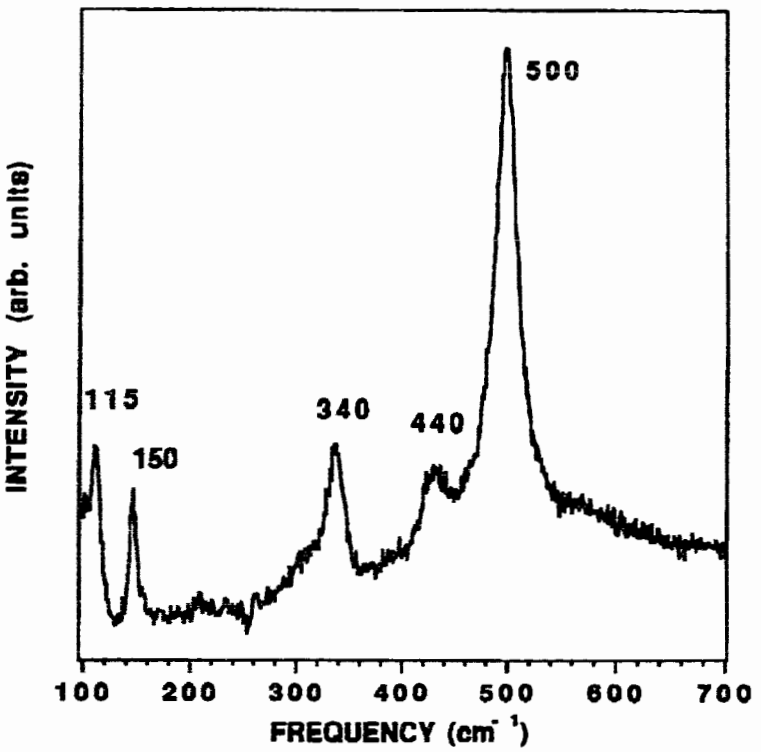

Figure 3.4 A spectrum from polycrystalline $YBa_2Cu_3O_7$.

For A_{1g} and B_{1g} modes the Raman tensors in tetragonal symmetry are

$$A_{1g} \begin{pmatrix} a & 0 & 0 \\ 0 & a & 0 \\ 0 & 0 & b \end{pmatrix} \quad \text{and} \quad B_{1g} \begin{pmatrix} c & 0 & 0 \\ 0 & -c & 0 \\ 0 & 0 & 0 \end{pmatrix} .$$

Therefore for the light polarized in the a-b plane (the polarization is perpendicular to c axis), the selection rules for A_{1g} and B_{1g} modes are $z(x'x')\bar{z}$ (or $z(y'y')\bar{z}$) and $z(x'y')\bar{z}$ respectively. In these notations, the first direction is the propagation direction of the incident light, the second the polarization direction of the incident light, the third the polarization direction of the scattered light and the fourth the propagation direction of the scattered light. $\bar{z}$ is the direction opposite to z-direction. x' is the unit vector along the diagonal between x- and y- axis, that is $x' = \frac{1}{\sqrt{2}}(1,1,0)$. Rotating x' by 90°, we get $y' = \frac{1}{\sqrt{2}}(-1,1,0)$. The coordinate system is shown in Fig. 3.5

3.2 Some Important Raman Scattering Results in $YBa_2Cu_3O_{7-x}$

3.2.1 The B_{1g} 340cm^{-1} Phonon Anomaly

There have been many reports on superconductivity induced changes in frequency and linewidth of the Raman active phonons related to the oxygen vibrations[33-35,52-54]. Among the three oxygen modes at 340cm^{-1}, 440cm^{-1} and 500cm^{-1}, the 340 cm^{-1} mode appeared to be very special. It has a very distinctive Fano shape which suggests an strong interaction between the phonon and an electronic continuum[13,19]. Its linewidth abruptly increases by up to 50% when an Y123 sample with x = 0.00 is cooled below T_c and the corresponding frequency decreases by about 8cm^{-1}.[35] The maximum linewidth

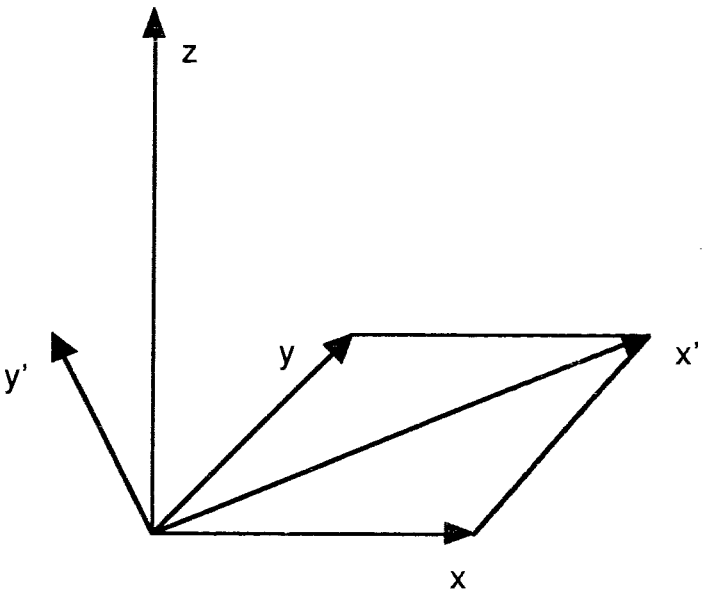

Figure 3.5 The coordinate system with **x// a** , **y//b** , **z//c** . **x'** is in the direction of (110) and **y'** is in the direction of (-1 1 0).

occurred at an ambient temperature 70K. For the sample with x = 6.93, the linewidth of the same mode first exhibits a small increase when T is lowered below T_c and then returns to a value expected on the basis of a simple anharmonic variation with temperature.[35] The decrease in frequency is also smaller. It seems that the behavior of the 340cm^{-1} mode is very sensitive to the doping level, or to the number of carriers in the CuO_2 planes. The 340cm^{-1} phonon anomaly and its doping dependence are summarized in Table 1. There $2\Delta\gamma = 2\gamma(\ 70K) - 2\gamma(\ 100K)$ and $\Delta\omega = \omega(20K) - \omega(100K)$.

Table 1 The 340cm^{-1} phonon anomaly and its doping dependence[35]

Sample	doping level	$2\Delta\gamma$	$\Delta\omega$
A	x = 0.00	~ 10cm^{-1}	~ 8cm^{-1}
B	x = 0.01	~ 5cm^{-1}	~ 6cm^{-1}
C	x = 0.07	~ 2cm^{-1}	~ 4cm^{-1}

As described in **1.3.2** Zeyher and Zwicknagl have attempted to model the phonon behavior in high T_c materials.[18] They found that when the phonon energy is slightly above the superconducting gap, the phonon's lifetime will be shortened because the phonon has sufficient energy to break a pair and hence the linewidth will be broadened below T_c .[22,23,18] When the phonon energy is lower than the gap value, it cannot break the superconducting pairs; the phonon can only decay through impurity scattering and the normal electron-phonon decay channel and since the free electron density is small for $T < T_c$

the phonon linewidth will be narrowed below T_c.[22,23] If the results of the experimental measurements are compared to the theoretical prediction by Zeyher and Zwicknagl, one finds a gap value around 340cm^{-1} for the sample with x =0.00 and 400cm^{-1} for x =0.07.[35] The gaps shift by about 18% ! Notice that when the oxygen concentration changes from 7.00 to 6.93 the transition temperature T_c only changes by 4K. In BCS theory, $\frac{2\Delta}{k_b T_c} = 3.5$ in the weak coupling limit. Even in the strong coupling limit, $\frac{2\Delta}{k_b T_c}$ is still a constant which is expected to be higher than 3.5. Since the difference in T_c is only 4.4% of T_c, the gap value should not change as much as indicated by the 340cm^{-1} phonon anomaly. Is the gap seen by the 340cm^{-1} phonon a superconducting gap? If it is, should it behave in this way?

3.2.2 The Behavior of The B_{1g} Raman Continuum

For the high T_c materials, there does not appear to be a cutoff at the high frequency end of the Raman continuum in either the superconducting or the normal state. The continuum goes at least to 10000cm^{-1} even in the normal state.[27-29] Chen et al [30] have carefully investigated the low energy portion ($\omega < 1200$cm^{-1}) of the continua and found:

(1) The A_{1g} continua peaked around 310cm^{-1} for both the samples with x =0.00, 0.01 and 0.07. The peak feature became clear at the ambient temperature 70K. At the ambient temperature 100K, there was no peak feature and the spectra were flat. The frequency distribution of the A_{1g} continuum appears to be consistent with the existence of a d-wave gap with a maximum value of $2\Delta \sim 310$cm^{-1}.

(2) The B_{1g} continua from the samples were quite different. For x=0.00 the B_{1g} continuum peaked around 470cm^{-1}, for x = 0.01 around 490cm^{-1} and for x = 0.07 around 550cm^{-1}. The low energy part of the B_{1g} continua was already somewhat depleted at the ambient temperature 100K. It was shown that the B_{1g} phonon couples with the B_{1g} continuum and the B_{1g} continuum itself is very sensitive to the doping level, therefore the B_{1g} phonon anomaly is also expected to be sensitive to the doping level.

There was also a report that the B_{1g} peak appeared even above T_c for a sample with x $\approx$0.30.[55] Somehow the report has not been confirmed. For the samples with lower oxygen concentration, the screening of the antiferromagnetic correlation in the CuO_2 planes is not complete. A doping dependent spin gap is expected at low temperatures, still higher than T_c, in the theory developed by Lee and Nagaosa.[56,57] Thus we have the question: is the B_{1g} continuum related to spin fluctuations? If it is, its doping dependence might be explained.(see the discussion in chapter 4)

3.2.3 The Anomalies in Phonon Intensities

The anomalies in phonon intensity in $YBa_2Cu_3O_{7-x}$ film were reported by Friedl et al.[41] The transition temperature of the film was 91K as measured by four-probe resistivity. The size of the grains in the film was of the order of 1μm observed with TEM. The c-axis was perpendicular to the film. The a- and b-axes of the grains were oriented rondomly in the film plane. The laser was focused to a point, roughly 50μm in diameter. Setting the polarizations of the incident and the scattered light to be parallel to each other, they measured the

intensity of the five A_{1g} phonons as a function of temperature between 300K and 10K. The 240cm^{-1} phonon intensity in BaF_2 at room temperature was used as the reference signal. All the phonon intensities were normalized to the reference signal. For the B_{1g} phonon, the obvious enhancement occurred immediately after the ambient temperature was decreased below T_c where the integrated phonon intensity increased by about a factor of two and this enhancement factor was independent of the laser wavelength. According to 2-11, this enhancement cannot be from the resonance of the laser frequency with a real intermediate state. Friedl et al[41] suggested that the enhancement was probably due to the resonance of the phonon energy with the superconducting gap as described by 2-14. For the A_{1g} phonon at 115cm^{-1}, the enhancements of the phonon intensity were dependent on laser wavelength of excitation. For the incident photons with energy 1.92eV and 2.60eV, the enhancement started almost exactly at an ambient temperature near T_c and the enhancement factor was almost the same, 2. For the incident photon with energy 2.34eV, the enhancement factor was less than 1.5. Again it was suggested that the enhancement of the 115cm^{-1} phonon's intensity was also from the resonance of the phonon energy with the superconducting gap by Friedl et al.[41] For the A_{1g} mode at 150cm^{-1}, they found the phonon intensity decreased after the ambient temperature was lower than T_c. For the A_{1g} modes at 440cm^{-1} and 500cm^{-1}, the error bars were too large to allow definitive conclusions but the data were qualitatively consistent with a superconductivity induced intensity enhancement.

Chapter 4
Experiment and Data Analysis

4.1 Experimental System

In the experiments presented here, a Spectra Physics model 165 argon ion laser was used to generate the incident beam with a wavelength at 514.5nm or 488.0nm. The incident beam was focused by two lenses and a right angle prism onto the sample. The scattered light was collected by a camera lens and focused onto the entrance slit of the spectrometer. The spectrometer used is a home built triple grating spectrometer. The first two gratings are couple in a subtractive dispersion mode to reject the laser line efficiently. The spectral dispersion is solely completed by the third grating. The dispersed light is directed onto a multi-channel detector allowing computer controlled data acquisition on all the channels simultaneously. The plasma lines from the laser were used for calibration purpose. The plasma lines have negligible linewidths when compared with the instrumental linewidth of about $3cm^{-1}$.

In the experiments, samples were mounted on a copper sample holder and enclosed in a dewar. The sample holder was connected to the cold finger. All the spectra were taken at a vacuum of about 10^{-3} Torr so that the Raman scattering due to air molecules can be removed. The vacuum was achieved by using rotary and diffusion pumps. An APD displex refrigerator was used for cooling and the lowest ambient temperature reached was 20K. The ambient temperature recorded for each spectrum was from the thermocurple at the end of the cold finger. A difference between the ambient temperature and the local temperature at the excitation spot on the sample is expected.

4.2 Sample Descriptions

The samples used in this experiment were lightly twinned high quality crystals of $YBa_2Cu_3O_{7-x}$ with $0.00 \leq x \leq 0.07$. The crystals were grown by R.Liang at UBC using a flux method as described elsewhere.[58] The different oxygen contents were estimated from the parameters used in the annealing conditions as described previously[59] and corroborated by x-ray diffraction measurements of the c-axis lattice parameter.[35] The transition temperatures were determined from magnetic susceptibility measurements. The information about the samples is summarized in Table.2. ΔT_c is the width of the transition region where the magnetic susceptibility as a function of temperature drops from 90% of its maximum to 10%, when a sample is cooled gradually to well below T_c.

Table 2 sample information

Samlpe	x	T_c(K)	ΔT_c(K)
A	0.00	89.7	2.5
B	0.01	92.8	0.8
C	0.07	93.7	0.2

In our experiment, the excitation was confined to a single domain of each sample. The spectra were equivalent to those from single crystals.

4.3 The Scattering Configuration

All the spectra were taken in a near back scattering geometry . The sample is oriented in such a way that its c-axis is perpendicular to the basal

plane of the sample holder and is defined as the z-direction. Both the incident and the scattered beams are not far away from the z-axis of the sample. The polarizations of the incident and scattered light are thus approximately parallel to the a-b planes of the sample. In this scattering geometry one can sample the xx, yy, xy and x^2-y^2 elements of the polarizability and the A_{1g} mode at 115cm^{-1} and B_{1g} mode at 340cm^{-1} both appear in the spectra with significant strength. For the A_{1g} modes at 150, 440 and 500cm^{-1}, however, the xx and yy elements of the polarizability are much smaller[45] than the zz component. As a result these modes appear relatively weakly in the spectra obtained here.

For A_{1g} spectra, the scattering configuration is $z(x'x')\bar{z}$ or $z(y'y')\bar{z}$; for B_{1g} spectra, $z(x'y')\bar{z}$. Typical spectra are shown in Fig. 4.1 and Fig. 4.2. In both Fig. 4.1 and Fig. 4.2, the intensity of the continuum is normalized to unity for $\omega \sim 700\text{cm}^{-1}$.

4.4 Measurement of Phonon Intensities

The integrated intensities of the phonons were all determined relative to the intensity of the continuum integrated over the region from 700cm^{-1} to 900cm^{-1} . To obtain the phonon intensity, the phonon spectral lineshape was determined by fitting the observed feature with either a Lorentzian profile for the symmetric A_{1g} phonons (at 150cm^{-1} and 440cm^{-1}) or a Fano profile for the asymmetric A_{1g} (at 115cm^{-1} and 500cm^{-1})and B_{1g} (at 340cm^{-1}) phonons. Thus for the symmetric phonons, we used

$$I(\omega) = B_0 + B_1\,\omega + A_1\frac{1}{(\omega-\omega_p)^2+\gamma^2} \qquad 4\text{-}1$$

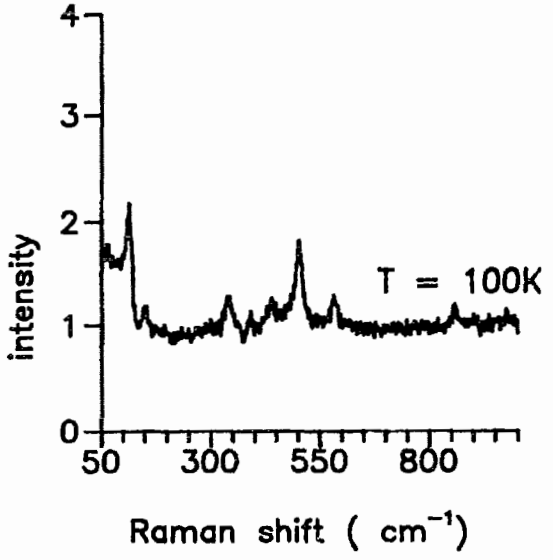

(a)

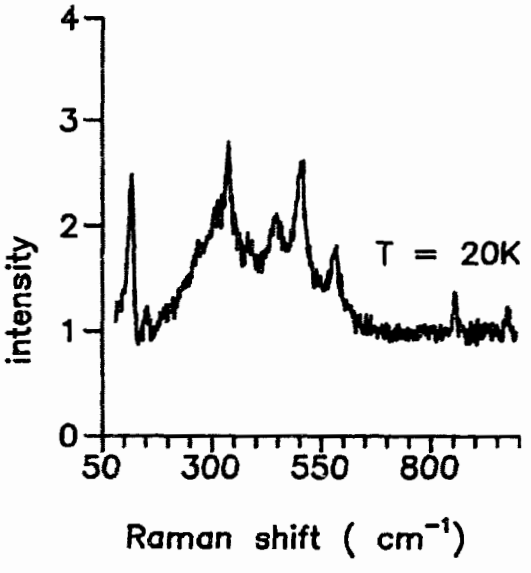

(b)

Figure 4.1 A_{1g} spectra from $YBa_2Cu_3O_{6.93}$ single crystal. The laser wave length used was 514.5 nm. The incident power was 6mW. The spectra have been normalized by setting the continuum intensity equal to unity at $\omega = 700cm^{-1}$.(a) at 100K and (b) at 20K.

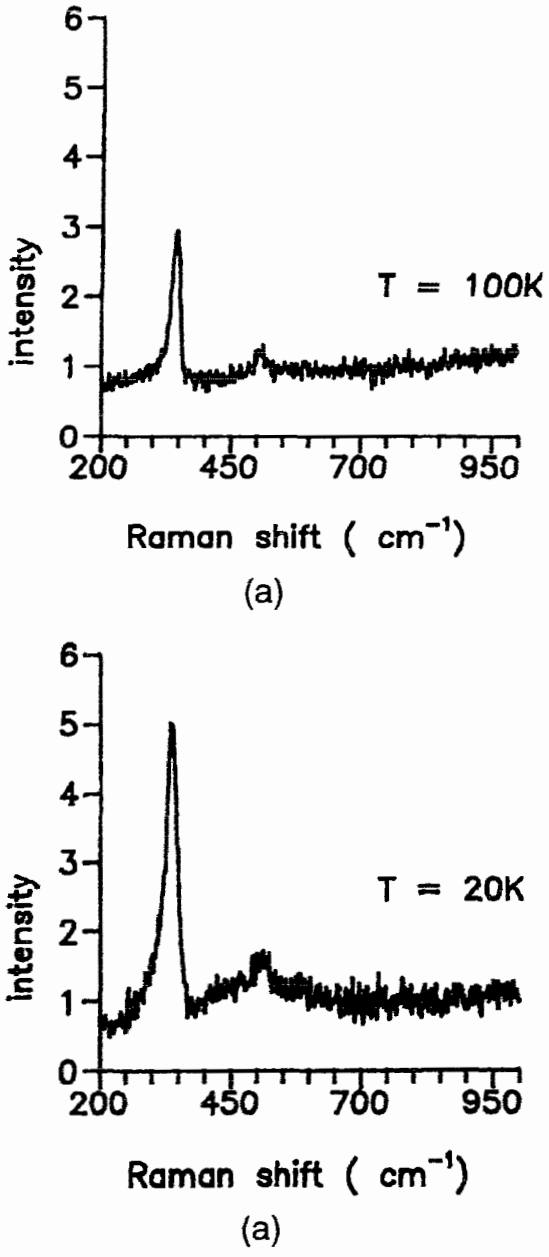

Figure 4.2 B_{1g} spectra from $YBa_2Cu_3O_7$ single crystal. The laser wavelength used was 514.5 nm and the incident power was 2mW. The spectra have been normalized by setting the continuum intensity equal to unity at $\omega = 700cm^{-1}$. (a) at 100K, (b) at 20K.

where B_0, B_1 and A_1 are all constants. B_0 and B_1 are used to account for any linear background that could be present. For the asymmetric phonons, the observed features were fit using

$$I(\omega) = B_0 + B_1\ \omega + A_2\frac{(\varepsilon+q)^2}{1+\varepsilon^2}\ . \qquad 4\text{-}2$$

The fitting results for 115cm^{-1} A_{1g} phonon and 340cm^{-1} B_{1g} phonon are shown in Fig. 4.3 and Fig. 4.4.

The integrated intensities for the phonons were then obtained by integrating over the profile obtained from the fitting procedure. It should be noted that any effects due to instrumental broadening were ignored, since for the 115, 340, 440 and 500cm^{-1} phonons the instrumental linewidth of about 3cm^{-1} was much less than the observed linewidths. The 150cm^{-1} phonon, however, has a width that is comparable to the instrumental width. No attempt was made to deconvolute the linewidth contribution since the 150cm^{-1} feature appears very weakly in the spectra. It is assumed that the 150cm^{-1} peak height serves as a measure of the phonon intensity in the spectra obtained.

As mentioned above, we took the Raman intensity of the continuum integrated over the region from 700-900cm^{-1} as the reference signal for determining an absolute number for the phonon intensity. Or in more detail, for the A_{1g} phonons, the reference signal was the Raman intensity of the A_{1g} continuum in the specified region; for the B_{1g} phonon, of the B_{1g} continuum. According to a previous report, the Raman intensities of the continua are temperature independent in the temperature region from 30-320K.[29] Since the phonon signal and the reference signal were necessarily from the same spot

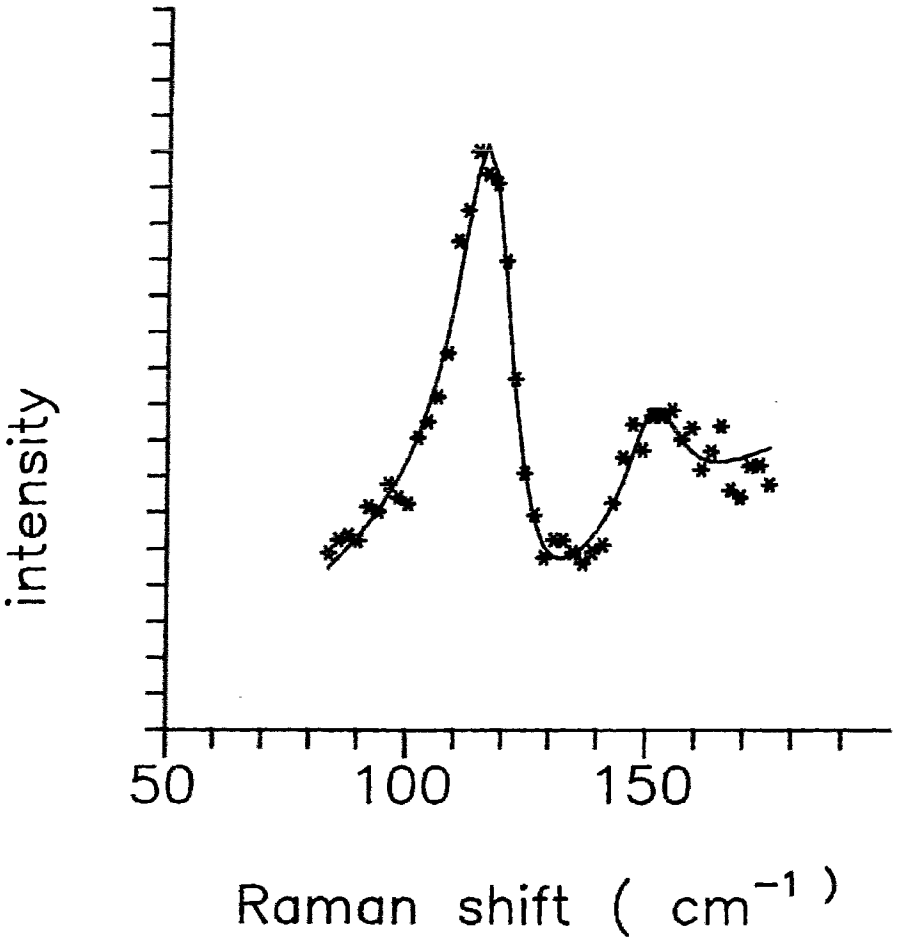

Figure 4.3 The fitting for the A_1g phonons at 115cm^{-1} and 150cm^{-1}. The spectrum was taken from $YBa_2Cu_3O_{6.93}$ at 20K. The laser wavelength used was 514.5nm. The power was 6mW. The intensity is in arbitrary units.

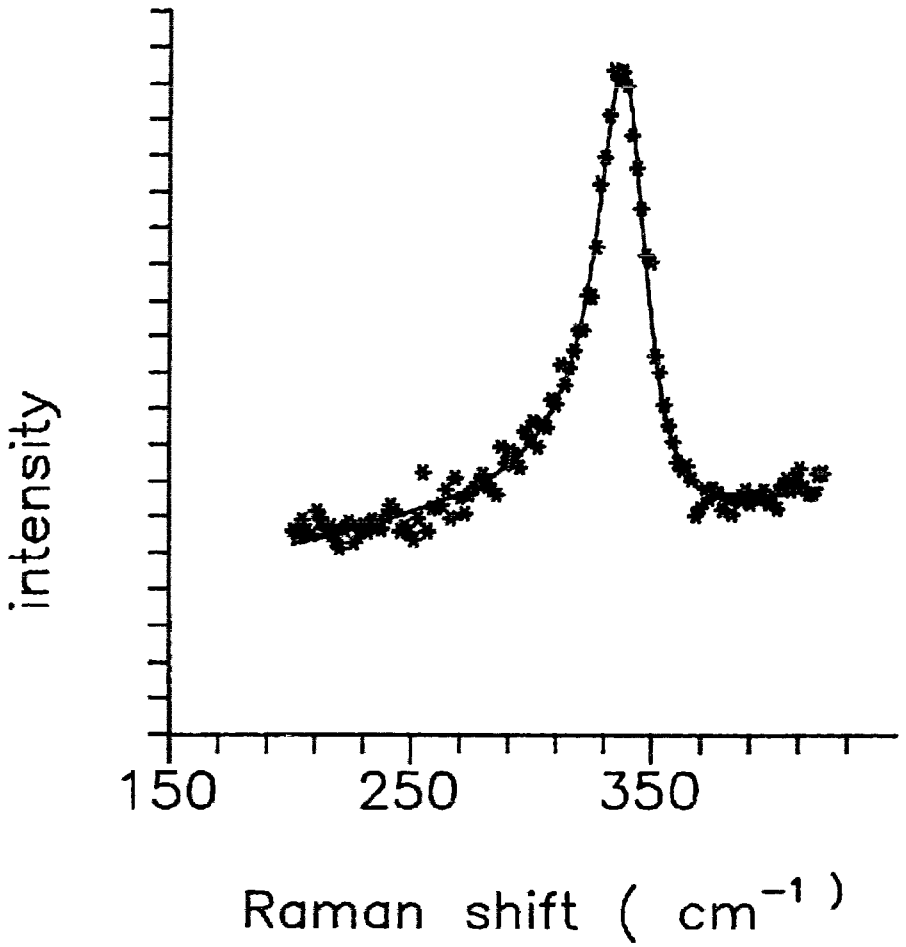

Figure 4.4 The fitting for the B1g phonon at 340cm^{-1}. The spectrum was taken from $YBa_2Cu_3O_7$ at 20K. The laser wavelength used was 514.5nm. The power was 2mW. The intensity is in arbitrary units.

of the sample, it could be safely assumed that the experimental conditions were the same for the two signals in any instant of time. Although the vibration of the cooling system may lead to the fluctuations in intensities, the ratio of the phonon intensity to the intensity of the continuum will not be affected.

We define the relative intensity of a phonon , I_R by

$$I_R = \frac{I_p}{\text{the intensity of the reference signal}} . \qquad 4\text{-}3$$

where I_p is the integrated intensity of the phonon. If the energy of a phonon is in resonance with a temperature dependent gap, the temperature dependence of the relative intensity of the phonon is proportional to $\frac{1}{(\omega p - \omega g(T))^2}$.

4.5 Experimental Results

4.5.1 Laser Heating Effects

In order to judge if a phenomenon is related to superconductivity or not, the onset temperature of the phenomenon is very important. We therefore wish the ambient temperature to be as close to the real sample temperature as possible. When the laser beam is incident on the surface of a sample, the heating caused by the laser beam creates a difference between the ambient and the local or effective temperature of the excited spot on the sample. We tried to minimize the laser heating effect by using a relatively low laser power of 6mW. The laser beam was focused by a spherical lens to a spot about 100 μm in diameter on the surface of the sample. For the laser power around 6mW, the power density was approximately 80W/ cm^2. To obtain an estimate for the

effect of laser heating the broadening of the 340cm^{-1} phonon in crystal A (x = 0.00) was measured with incident powers of 2mW and 6mW. Briefly, if a fuily oxygenated sample of Y123 is cooled below T_c, the B_{1g} phonon at 340cm^{-1} is observed[35] to suddenly broaden by about 50%. To estimate the effect of laser heating the ambient temperatures of the onset of broadening and the ambient temperatures at which maximum broadening occured were compared for the two different power levels (Fig. 4.5). It was found that the difference between the temperatures was approximately 10K. Thus the use of 6mW incident power increases the sample temperature in the incident area by about 10K.

To obtain an alternate indication of any effect due to laser heating the intensity enhancement of the B_{1g} phonon was also measured using incident powers of 2mW and 6mW. The results obtained are shown in Fig. 4.6(a) and Fig. 4.6(b). It is clear that the two sets of data are very similar. In other words the results are not altered in any significant way by using 6mW incident power. Thus, finally, to account for the effect of laser heating all ambient temperatures were simply shifted by 10K when using 6mW of incident power.

4.5.2 The B_{1g} Phonon Intensity Enhancement

Fig. 4.6 shows the relative intensities of the B_{1g} phonon as a function of temperature for the sample A (x = 0.00). The data used in obtaining the results in Fig. 4.6(a) were obtained from spectra excited using the 514.5nm line of the A_r^+ laser and 6mW of incident power; the results in Fig. 4.6(b) were obtained with 2mW of incident power at the same wavelength. Fig. 4.6(c)

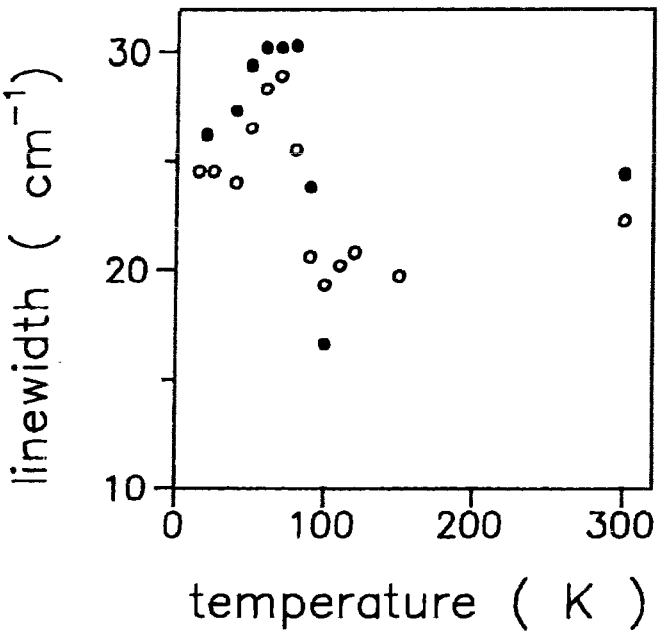

Fig. 4.5 The broadening of the linewidth of the B_{1g} phonon at 340cm^{-1} when crystal A (x = 0.00) is cooled below T_c. The excitation laser wavelength is 514.5nm. The data represented by the open circles were obtained by using an incident power about 6mW. Another set of data (solid dots) were obtained by using an incident power around 2mW.

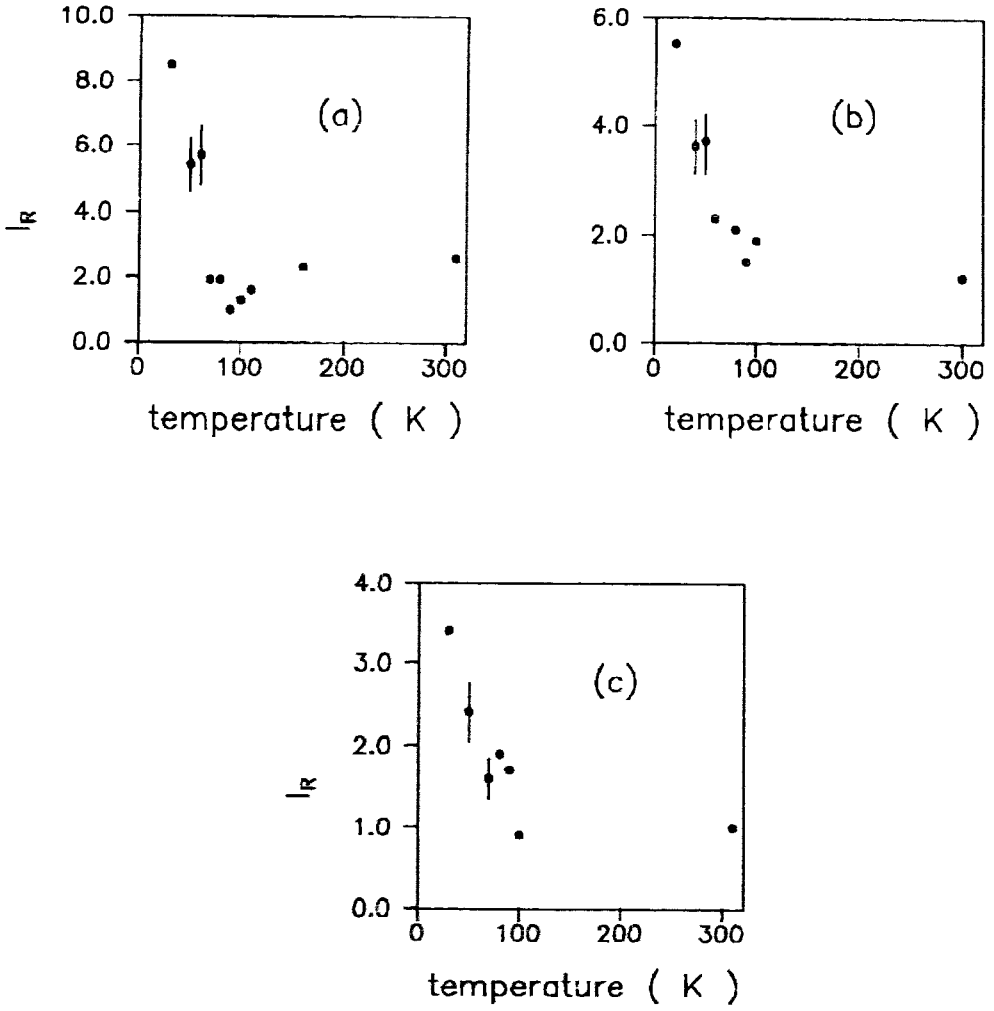

Figure 4.6 The enhancement of the B_{1g} phonon intensity in $YBa_2Cu_3O_7$ measured with (a) $\lambda = 514.5$nm at 6mW, (b) $\lambda = 514.5$nm at 2mW and (c) $\lambda = 488.0$nm at 6mW. The normalization of the relative intensity scale has been chosen arbitrarily. The uncertainty in the value of I_R is about 15%.

presents the results obtained using the 488.0nm line of the A_r^+ laser and 6mW of incident power. It is clear from Fig. 4.6 that if we define the intensity enhancement factor by the ratio of the relative intensity at the lowest temperature reached to the average value of the relative intensities at normal phase (except for the point where T is very close to T_c),the superconductivity induced enhancement is about a factor of 4 ± 0.7 for all these sets of excitation conditions. An unexplained feature of these results is that the onset temperature of the superconductivity induced intensity enhancement appears to be marginally higher for the 488.0nm data than for the 514.5nm data. This appears to indicate that the local laser heating is reduced by using λ= 488.0nm excitation.

The relative intensities of the B_{1g} phonon as a function of temperature are shown in Fig. 4.7 for the sample C (x = 0.07). The data obtained using an excitation wavelength of 514.5nm are shown in Fig. 4.7(a) and the results shown in Fig. 4.7(b) were obtained from the spectra using λ = 488.0nm excitation. It is clear from Fig. 4.7 that the intensity enhancement of the B_{1g} phonon in this crystal is much weaker than that for the x = 0.00 crystal. From the data it is estimated that the superconductivity induced enhancement in the intensity of the B_{1g} phonon is about a factor of 1.8 ± 0.3 in the x = 0.07 sample. Again in the x = 0.07 sample the data obtained with the 488.0nm line yield an onset temperature for the superconductivity induced intensity enhancement that is slightly higher than for the data obtained with λ = 514.5nm. For all the three samples, the relative intensities of the B_{1g} phonon obtained with the excitation wavelength λ = 514.5nm and an incident power of

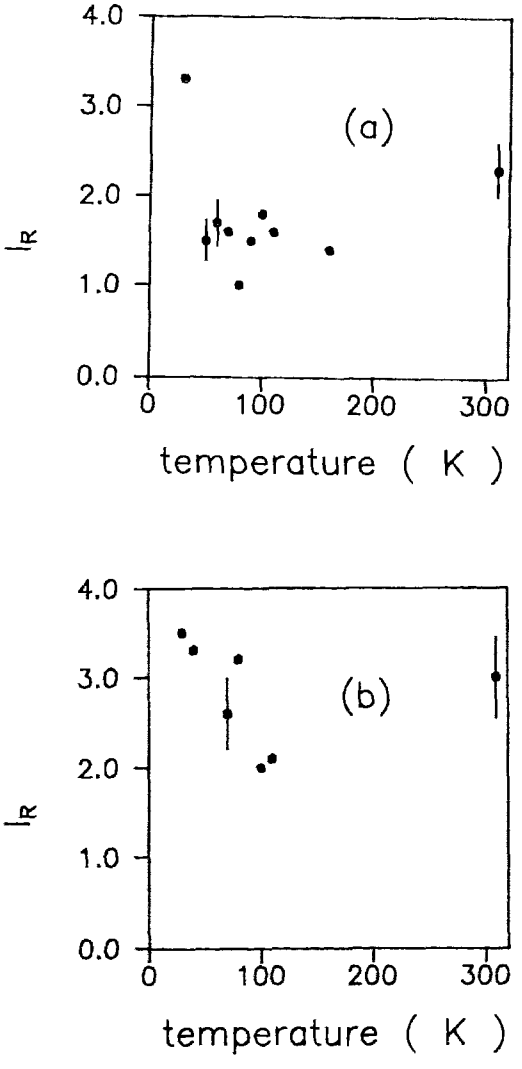

Figure 4.7 The enhancement of the B_{1g} phonon intensity in $YBa_2Cu_3O_{6.93}$ measured with (a) $\lambda = 514.5$nm at 6mW and (b) $\lambda = 488.0$nm at 6mW. The normalization of the relative intensity scale has been chosen arbitrarily. The uncertainty in I_R is about15%

6mW are shown in Fig. 4.8 as a function of temperature. From this figure it is evident that the enhancement decreases from about 4±0.7 for crystal A to 1.8±0.3 for crystal C. Thus we must conclude that the superconductivity induced enhancement in the B_{1g} phonon intensity is very sensitive to the doping level. On the other hand, the enhancement is independent of the laser wavelength within our experimental uncertainty.

4.5.3 The A_{1g} Phonon Intensities

Because the scattering geometry used in these experiments had the incident and scattered light polarized in the a-b plane of the crystal, the intensities of the 150,440 and 500cm^{-1} A_{1g} oxygen vibrations appear[45] quite weakly in the spectra and the 115cm^{-1} phonon is the only A_{1g} mode that appears with significant strength. Thus reliable data could be obtained for the relative intensity of the 115cm^{-1} mode and results are presented in Fig. 4.9 as a function of temperature. The superconductivity induced enhancement obtained from these data is about a factor of 2±0.3 for all three crystals.

The relative intensities of the 440 and 500cm^{-1} A_{1g} modes are shown in Fig. 4.10 as a function of temperature for all three samples. As mentioned above these features appear weakly in the spectra, the uncertainty associated with the data is large (~ 30%). Thus the superconductivity induced intensity enhancement cannot be accurately estimated. It appears that there is an approximate enhancement of a factor of 2±0.7 for each phonon and that within the experimental uncertainty there is no dependence on oxygen concentration in this doping range ($0 \leq x \leq 0.07$).

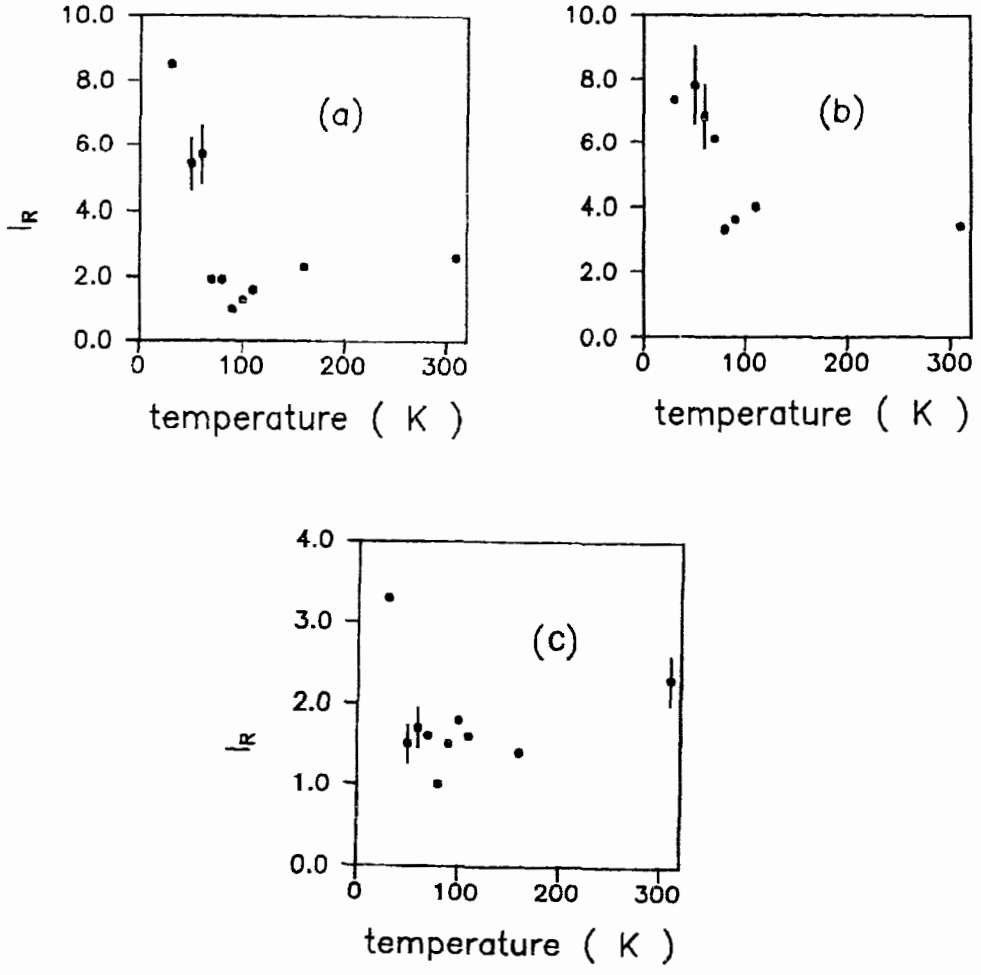

Figure 4.8 The enhancement in the intensity of the B_1g phonon in $YBa_2Cu_3O_{7-x}$ with different oxygen content. (a) x = 0.00, (b) x = 0.01and (c) x = 0.07. All the data were obtained by using an excitation wavelength λ = 514.5nm and the incident power was 6mW. The normalization of the relative intensity scale has been chosen arbitrarily. The uncertainty in I_R is about 15%.

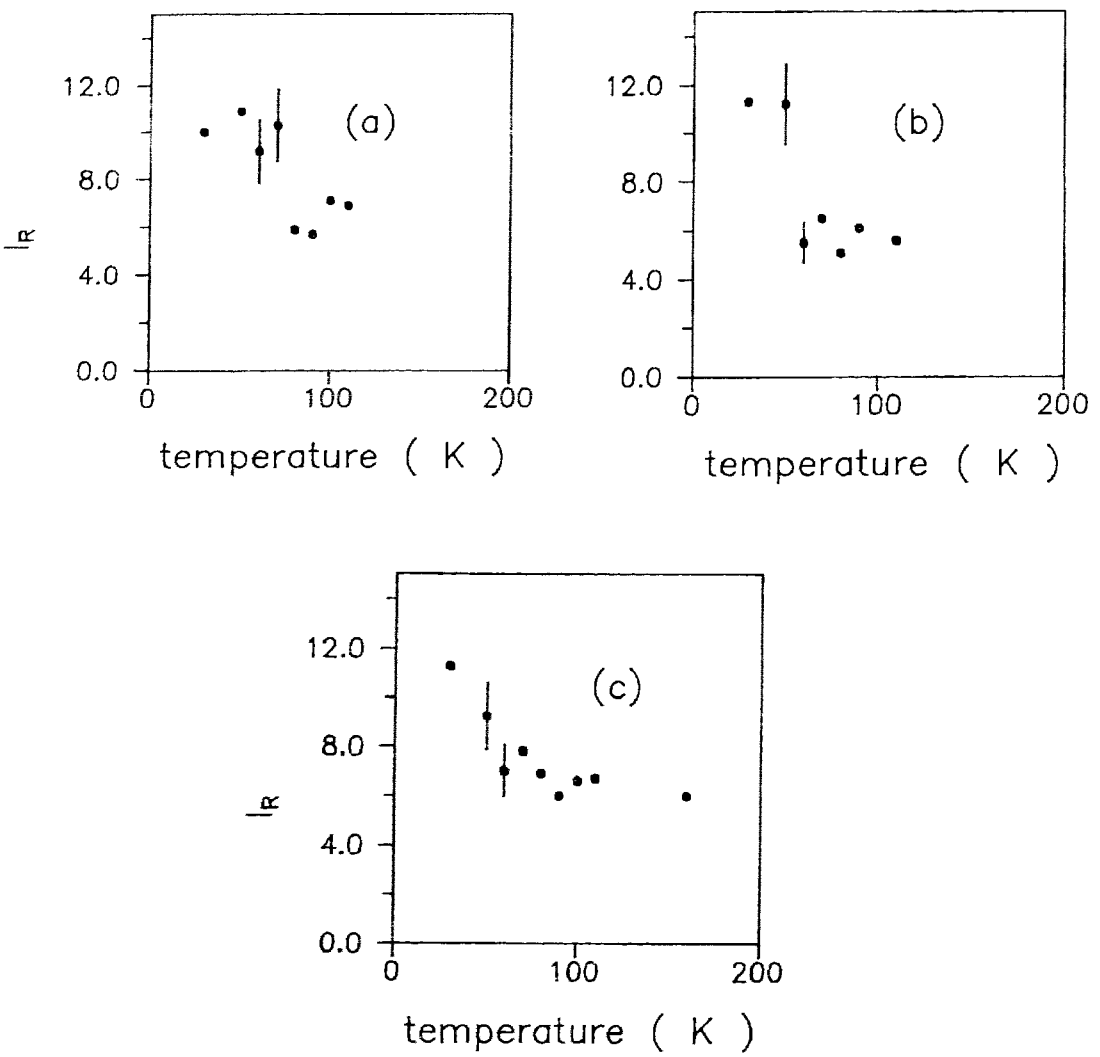

Figure 4.9 The enhacement in the intensity of the A_{1g} phonon at 115cm^{-1} in $YBa_2Cu_3O_{7-x}$ with different oxygen content. (a) x = 0.00, (b) x =0.01 and (c) x = 0.07. All the data were obtained by using an excitation wavelenght λ = 514.5nm and the incident power was 6mW. The normalization of the relative intensity scale has been chosen arbitrarily. The uncertainty in I_R is about 15%.

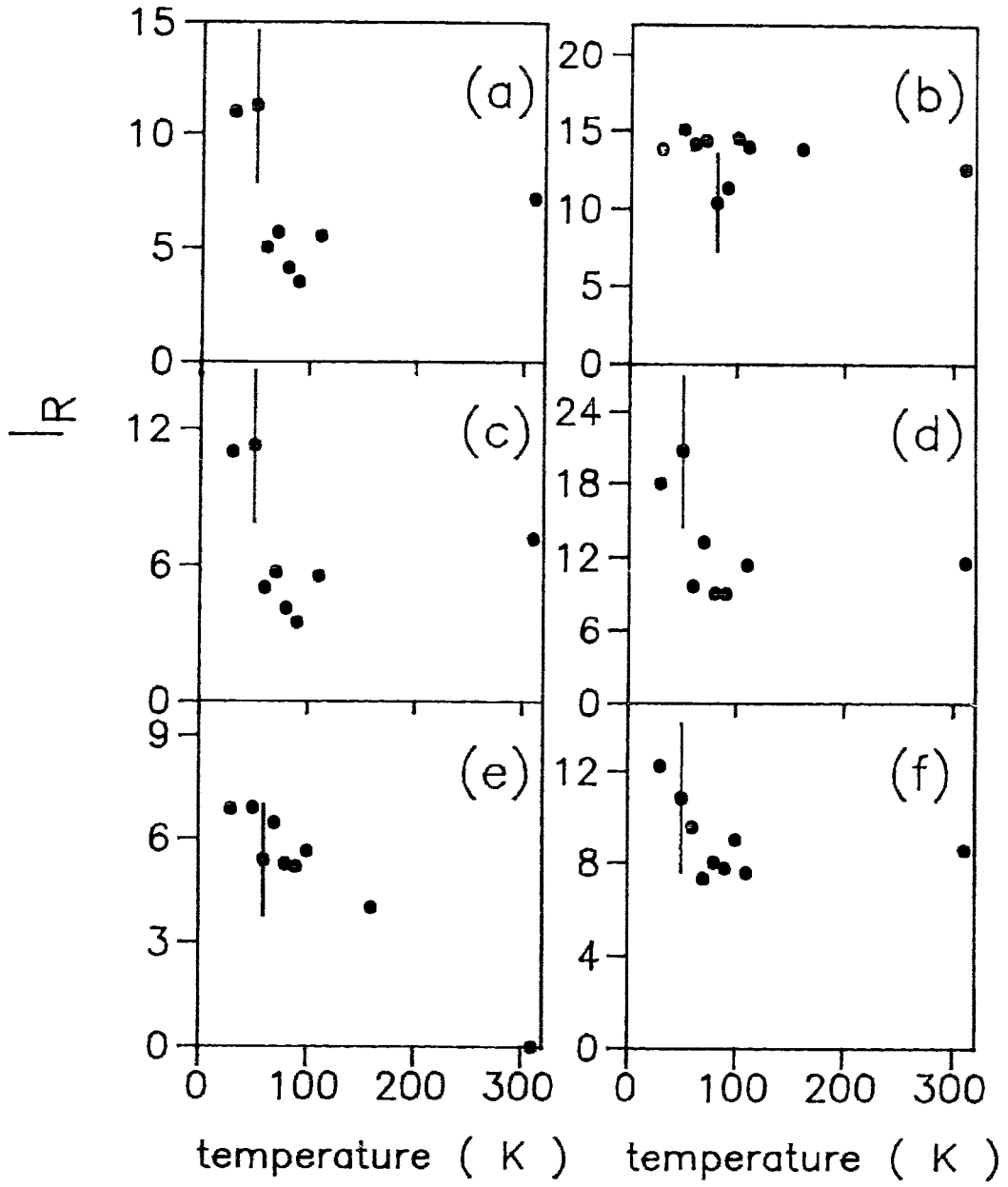

Figure 4.10 The enhancement in the intensities of the A_{1g} phonons at 440 and 500cm^{-1} in $YBa_2Cu_3O_{7-x}$ with different oxygen content. All the data were obtained by using an excitation wavelength $\lambda = 514.5$nm. The incident power was 6mW. The normalization of the relative intensity scale has been chosen arbitrarily.

(a) x = 0.00 and $\omega = 440$cm^{-1}. (b) x = 0.00 and $\omega = 500$cm^{-1}.

(c) x = 0.01 and $\omega = 440$cm^{-1}. (d) x = 0.01 and $\omega = 500$cm^{-1}.

(e) x = 0.07 and $\omega = 440$cm^{-1}. (f) x = 0.07 and $\omega = 500$cm^{-1}.

The results of the 150cm^{-1} mode are shown in Fig. 4.11 for all three samples. As mentioned above the accuracy of these measurements is limited by the weakness of this mode in the basal plane spectra and further complicated by the fact that it has a narrow linewidth that is comparable to or smaller than the apparatus width of about 3cm^{-1} as mentioned previously. We have not attempted to deconvolute the line profile because of the weakness of the feature and then the points in Fig. 4.11 should be considered to simply represent a measure of the peak height of the 150cm^{-1} feature in different spectra.

4.6 Discussion of Experimental Results

4.6.1 Comparison to Previous Work.

As mentioned previously Friedl et al[41] have carried out a study of the superconductivity induced phonon intensity enhancements in Y123. For the excitation wavelengths λ = 530.9nm and λ = 476.2nm, their results are shown in Fig. 4.12. The results presented here support their findings as following:

(1) The B_{1g} phonon exhibits the largest superconductivity induced intensity enhancement of all the phonons.

(2) The B_{1g} phonon enhancement is independent of the exciting wavelength within the experimental uncertainty and the enhancement is similar in magnitude to that found in Ref. 41.

(3) The 115cm^{-1} A_{1g} phonon exhibits a superconductivity induced intensity enhancement of about a factor of 2±0.3 for λ = 514.5nm. It is in agreement with Ref. 41.

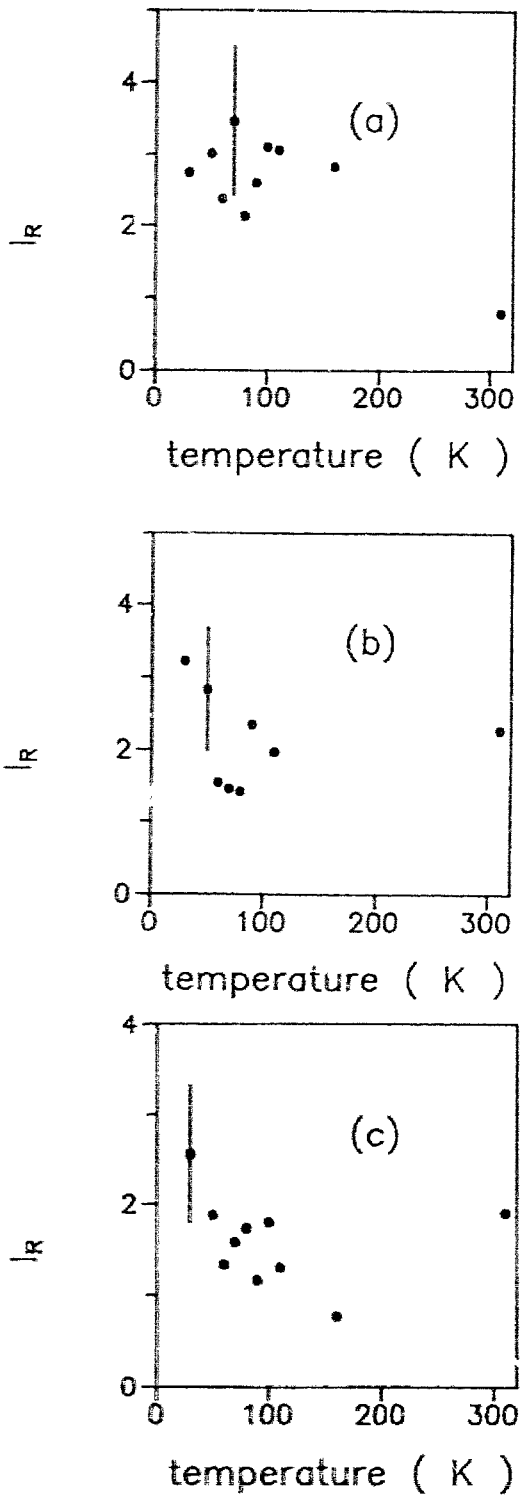

Figure 4.11 The intensity enhancement of the A_{1g} phonon at 150cm^{-1} in $YBa_2Cu_3O_{7-x}$ with different oxygen content. All the data were obtained by using an excitation wavelength λ =514.5nm. The incident power was 6mW. The normalization of thr relative intensity scale has been chosen arbitrarily.(a) x = 0.00, (b) x = 0.01 and (c) x = 0.07

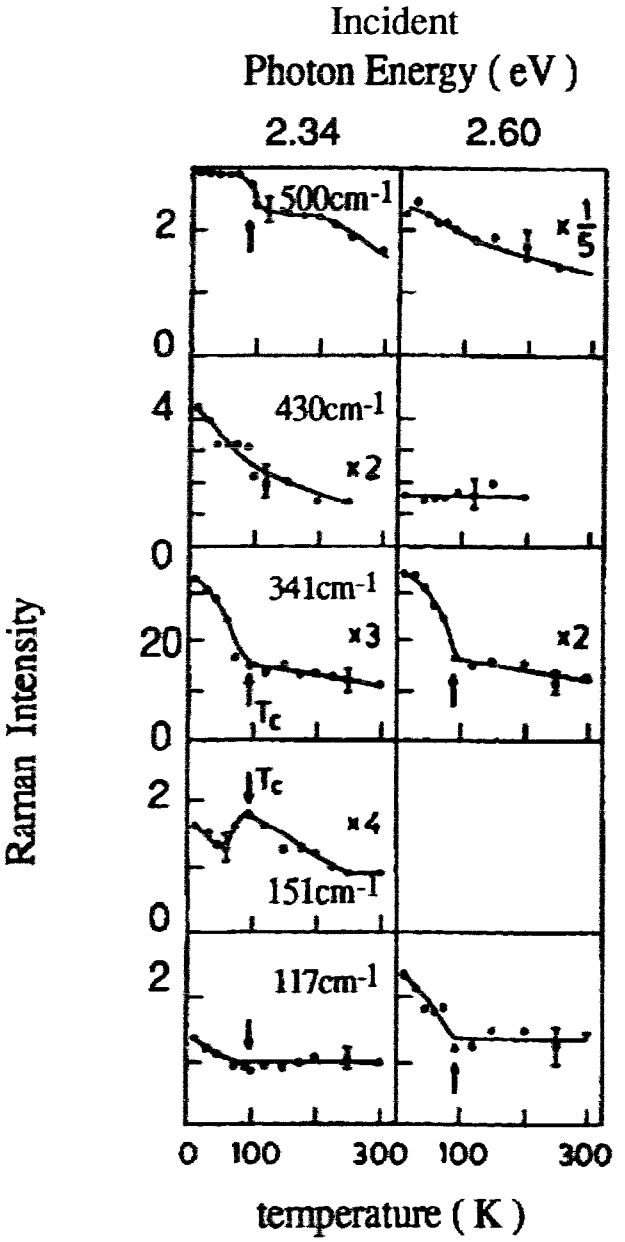

Figure 4.12 Ramam intensities of the five Ag phonons of $YBa_2Cu_3O_{7-x}$ as a function temperature and for two different excitation energies.

(taken from Ref. 41)

(4) As can be seen from a comparison of our data (Fig. 4.6 - Fig. 4.11) with those of Friedl et al (Fig. 4.12) there are minor discrepancies between the two sets of data. This is perhaps to be expected in that our results were obtained from high quality crystals and the A_{1g} modes ($\omega > 150cm^{-1}$) were very weak, whereas in the spectra obtained by Friedl et al[41] from a c-axis oriented film the A_{1g} modes at 150, 440 and $500cm^{-1}$ are all relatively strong. This indicates that there is a significant c-axis contribution to their spectra and hence their film must be somewhat polycrystalline.
(5) Friedl et al[41] observed a negtive enhancement (Fig. 4.12) for the $150cm^{-1}$ mode just below T_c. There is perhaps some indication of this decrease in intensity below T_c in our data (Fig. 4.11). We believe, however, that the measurements of Friedl et al of the $150cm^{-1}$ mode probably suffer the same resolution limits that are inherent in our results, although they did not remark on this aspect. Thus we would suggest that all measurements of the $150cm^{-1}$ phonon are particularly suspect.

4.6.2 Doping Dependence of The B_{1g} Phonon Intensity Enhancement

It is clear that the superconductivity induced intensity enhancement of the B_{1g} phonon is much smaller in crystal C (x = 0.07) than in crystal A (x = 0.00). To obtain an explanation we must review the physical reason responsible for the enhancement. Friedl et al[41] suggested that the enhancement arose because of a resonance between the phonon and a single sharp superconducting gap. The B_{1g} phonon, which was assumed [11,12,18] to have an energy near the gap, would thus exhibit the largest effects. Although

we no longer believe that there is a single sharp gap in Y123, let us pursue this resonance mechanism further.

Let us assume, following Friedl et al[41], that the superconductivity induced intensity enhancement can be attributed to a resonance between the phonon energy and the superconducting gap. First let A represent the scattering processes that are present both before and after the formation of the superconducting gap. Then the resonance term associated with scattering across the superconducting gap will be given by 2-14 and from 4-3 we have

$$\frac{I_R\,(\,T < T_c\,)}{I_R\,(\,\text{normal}\,)} \cong \frac{A + \dfrac{B}{(\omega_p - \omega_g)^2}}{A}. \qquad 4\text{-}4$$

We assume, given the results of the phonon anomaly experiments,[17] that the phonon energy is very close to a gap energy for the x = 0.00 sample and choose $|\omega_g - \omega_p| \sim 0.1\ \omega_p$ as a reasonable estimate.[11] Thus from 4-4 with

$\dfrac{I_R\,(\,30K\,)}{I_R\,(\,\text{normal}\,)} \approx 4$, we obtain $\dfrac{A}{B} \approx \dfrac{33}{\omega_p^2}$.

Now assume that A and B are independent of doping (no big change in band structure) for $0.00 \le x \le 0.07$. Setting the intensity ratio in 4-4 equal to 2 for the x = 0.07 crystal, we obtain $\omega_g - \omega_p \sim 60\text{cm}^{-1}$. That is the " gap " seen by the B_{1g} phonon appears to increase as oxygen is removed from the crystal and the resonance between the ω_p and ω_g becomes weaker, leading to a smaller superconductivity induced intensity enhancement. The smaller resonance factor leads to a very rough estimate of $90 \pm 30\text{cm}^{-1}$ for the actual increase in the magnitude of the gap. Despite its roughness, however, this

result is in both qualitative and quantitative agreement with the previous results for the B_{1g} " gap " shift as deduced from B_{1g} phonon anomaly measurements and direct observation of the B_{1g} continuum. Both these measurements indicate a 60 to 80cm^{-1} shift of a B_{1g} " gap " to higher energy when x is changed from 0.00 to 0.07. In this context one can thus view the present results as confirmation of the enhancement mechanism proposed by Friedl et al[41] , namely a resonance between the B_{1g} phonon energy and the energy of a " gap " in the B_{1g} continuum.

4.6.3 Superconductivity Induced Intensity Enhancement of The A_{1g} Phonons.

As noted in the previous sections the 115, 150, 440 and 500cm^{-1} phonons all exhibit a superconductivity induced intensity enhancement of about a factor of two in all three crystals. It has also been remarked that the three most energetic features are weak and this introduces a large uncertainty (~ 30%) into the value estimated for the enhancement. The data however do suggest, and are certainly not incompatible with, a superconductivity induced intensity enhancement that is between 1.5 and 2. In fact in spectra obtained from most crystals the 440cm^{-1} mode becomes observable only at low temperatures. We also know (section 1.4.2) that the A_{1g} phonons interact with the A_{1g} continuum. Furthermore assume that this continuum can be characterized by a clean gap with $2\Delta \sim 310cm^{-1}$ and that the superconductivity induced intensity enhancement again arises from a resonance between each phonon and the gap. Then given the energy of each phonon relative to a gap energy of 310cm^{-1}, one

would anticipate approximately the same enhancement for each of the phonons. In addition a factor of 1.5 to 2 is perhaps quite reasonable , given that the factor A in 4-4 would in this case be relatively small for all the phonons except the 115cm^{-1} mode.

For a clean gap, however, one might expect to see the intensity of the 115 and 150cm^{-1} modes go through a maximum as the gap opens below T_c. In this case the maximum would occur at that temperature when the gap energy is equal to the phonon energy. There is no indication of any such resonant maximum in the data shown in Fig. 4.9 and Fig. 4.11. Friedl et al [41] have suggested that such singularities might vanish in the strong coupling limit. This should however also lead to a vanishing of the phonon anomalies which have in fact been clearly observed for the 115cm^{-1} mode.[36] An alternate explanation might be found if one invokes the existence of a d-wave gap as is suggested by the low energy excitations in the A_{1g} continuum (Fig.1.7).

Recently, Pines and coworkers[60] suggested that the pairing mechanism in high temperature superconductors was spin fluctuation induced, and then showed that if this was the case the superconducting gap must have $d_{x^2-y^2}$ symmetry. That is the magnitude of the gap in momentum space should be given by

$$2\Delta = 2\Delta_0 (\cos k_x a - \cos k_y a) . \qquad 4\text{-}5$$

This gap has nodes on the Fermi surface along the lines ($1\bar{1}0$) and has its maximum value along the directions (100) and (010). Some recent experiments have provided results in agreement with such a gap[61] and in fact the A_{1g} continuum in Fig. 1.7 is well reproduced if scattering across such a gap is assumed.[38]

Thus given such a d-wave superconducting gap with a maximum value of $2\Delta_{max} \cong 310cm^{-1}$, there always exist some regions on the Fermi surface where the magnitude of the gap value is around $115cm^{-1}$ at $T<T_c$. In these regions, which may constitute a relatively small portion of the Fermi surface, the $115cm^{-1}$ phonon will be in almost exact resonance with the gap. Moreover as the temperature of the sample is lowered below T_c the resonant enhancement should increase in a more or less continual manner, as more and more of the Fermi surface contributes to the enhancement. The steady increase in the superconductivity induced enhancement that is observed for both the $115cm^{-1}$ and $150cm^{-1}$ modes , as T is reduced below T_c, could be interpreted as being qualitatively consistent with the existence of a superconducting gap with a d-wave symmetry. Similarly, the enhancements of the phonon intensity for A_{1g} phonons at $440cm^{-1}$ and $500cm^{-1}$ expected for a d-wave gap with $2\Delta_{max} = 310cm^{-1}$ should be similar to that expected for a sharp gap of the same magnitude and thus these factor of 1.5 to 2 can also be considered to be comsistent with a d-wave gap picture. As a final remark concerning the existence of a d-wave gap in Y123 it should be noted that E.J.Nicol et al[62] have extended the work of Zeyher and Zwicknagl (ZZ)[18] and provided a more accurate calculation of the phonon anomalies one should observe as a sample is cooled below its critical temperature. They[62] found, in contrast to ZZ[18], that given an s-wave or symmetric gap, a phonon cannot both soften and broaden. On the other hand, given a d-wave gap, this simultaneous softening and broadening becomes possible.[62] Thus since the B_{1g} phonon is observed to both broaden and soften in Y123 this could be interpreted as support for a d-wave gap in Y123.

4.6.4 Is The B_{1g} " Gap " Related to Spin Fluctuation ?

As we have seen in the previous sections the intensity enhancements of the A_{1g} phonons can be viewed as being consistent with the existence of a d-wave gap with $2\Delta_{max} = 310cm^{-1}$. As noted previously the observed frequency distribution in the A_{1g} continuum is also well reproduced[38] by a theoretical calculation of scattering across a d-wave gap. However the B_{1g} phonon behavior does not appear to be consistent with this picture. As described in section 4.5.2 the rapid decrease in the B_{1g} phonon intensity enhancement with increasing x implies that the " gap " associated with the B_{1g} continuum increases by about 30% (from 315 to $400cm^{-1}$) as x is changed from x = 0.00 to x = 0.07. It should be remembered that T_c changes by only 4% in this same concentration region and the Fermi surface[37] is expected to be very similar for all compounds in this concentration region. Furthermore , this increase in the B_{1g} " gap " is supported by phonon anomaly measurements[35] and direct observation of the electronic B_{1g} continuum.[30] It is difficult to imagine how 2Δ could change by 30% while T_c remains roughly constant and thus it seems reasonable to question the origin of the B_{1g} " gap ".

Let us pursue the possibility that the gap feature in the B_{1g} continuum is not only related to superconductivity but also to something else. We speculate that the B_{1g} feature perhaps contains two components, one is related to a superconducting gap and the other to a spin gap. For the oxygen concentration in the region from x = 1.00 to 0.56, the static antiferromagnetic correlation in the CuO_2 planes has been shown to exist.[63] For oxygen concentration larger than 6.45, the static long range antiferromagnetic correlation is destroyed

completely, but the dynamic antiferromagnetic correlation persists even into the superconducting phase.[64,65] As pointed out by Nagaosa and Lee,[56,57] a spin gap may develop above T_c for the underdoped materials . The temperature dependence of a spin gap Δ_S can be described by

$$\Delta_S \sim J|T-T_d|^{\frac{1}{2}}, \qquad 4\text{-}6$$

where J is the exchange energy which is a function of the oxygen concentration and T_d is the transition temperature for the formation of paired spinons(the topological defects with spin 1/2 and zero charge in the RVB theory). T_d increases with decreasing of oxygen content. For the superconducting materials with low oxygen content, the spin gap could thus be significantly larger than the superconducting gap. Since $T_d > T_c$, thus anomalies related to the spin gap could occur above T_c.[66] Once the superconducting gap opens, the superconducting gap will dominate in the response functions of the material.[56] For doping levels close to the optimal doping, x = 0.00 for Y123, the spin gap value could be just slightly larger than the superconducting gap and an anomaly related to the spin gap could also occur near T_c. The response functions of the material will be determined by these two different kinds of gaps. This is just the case of our samples. From 4-6 we know that the spin gap is doping dependent. The larger the oxygen deficiency, the larger the spin gap. The doping dependence of the spin gap is consistent with the shift of the B_{1g} peak position to a higher value, when the oxygen concentration decrease from x = 0.00 to 0.07. If the B_{1g} feature does have some relation with the spin gap, then the spin gap is very sensitive to the

oxygen concentration. Since J is of the scale of electronic energy, a small change in T_d could lead to an appreciable shift in the spin gap value. The sensitive dependence of the B_{1g} phonon anomaly, the peak position of the B_{1g} continuum and the intensity enhancement of the B_{1g} phonon to the doping level can be explained . Recently, there was a report about the B_{1g} phonon anomaly around 110K in the sample with x = 0.05.[67] For the sample with x = 0.05, T_c is 93K with ΔT_c=0.3K. If the result is further confirmed, it could be a strong argument in favor of the spin gap related anomaly of the B_{1g} phonon. In our experiment, we haven't observed any phonon anomaly or intensity anomaly well above T_c for the B_{1g} phonon in Y123 crystal with x = 0.00 and 0.07.

Chapter 5 Conclusions

Raman Scattering experiments have been carried out on three single crystals of $YBa_2Cu_3O_{7-x}$ with x = 0.00, 0.01 and 0.07. The intensities of the five Raman active phonons with c-axis vibration were measured as a function of temperature in Raman spectra obtained from all three samples. The intensity of the B_{1g} phonon was also measured as a function of laser wavelength. The results, which are summarized in the following sections, indicate that the superconductivity induced intensity enhancement of the phonons occurs because of the interactions between the phonons and electronic excitations across a gap that opens below the superconducting transition temperature T_c.

5.1 The Enhancement in The Intensity of The A_{1g} phonons

It was found that the intensity of the A_{1g} phonon at 115cm^{-1} (Ba vibrations) increased by a factor of 2±0.3 when the samples were cooled below T_c. The intensity enhancement had an onset temperature very near T_c in all samples and the magnitude of the enhancement was independent of oxygen concentration x for $0 \leq x \leq 0.07$.

For the other A_{1g} phonons at 150, 440 and 500cm^{-1}, their intensities were quite weak. The superconductivity induced intensity enhancement below T_c was again estimated to be about 1.5 to 2, but the experimental uncertainty in these results is large (~ 30%).

If we assume that the enhancement in the intensity of the A_{1g} phonon at 115cm^{-1} is due to an interaction between the phonons and excitation across the

superconducting gap, then it should also follow that the superconducting gap does not change with x for $0 \leq x \leq 0.07$. This is in agreement with direct measurements of the A_{1g} continuum, which is assumed to provide a measure of the superconducting gap value and is the same for all three samples with x = 0.00, 0.01 and 0.07. Furthermore the intensity anomalies of the 440 and 500cm^{-1} phonons are independent of the oxygen concentration for $0 \leq x \leq 0.07$ and are thus also consistent with a constant value for 2Δ. The results for the superconductivity induced intensity enhancement of all the A_{1g} phonons are thus consistent with phonon anomaly measurements[35] and A_{1g} continuum studies[30] which also imply that the A_{1g} gap is independent of doping for $0 \leq x \leq 0.07$. The magnitude and temperature dependence of the A_{1g} phonon intensity enhancements, in particular the 115cm^{-1} mode, are qualitatively consistent with calculations[38] which suggest that the superconducting gap has d-wave symmetry.

5.2 The Enhancement in The Intensity of The B_{1g} Phonon

The B_{1g} phonon exhibited a stronger superconductivity induced intensity enhancement than did the A_{1g} phonons. For sample A (x = 0.00) the measured intensity enhancement was 4.0 ± 0.7 when the sample was cooled below T_c. The superconductivity induced enhancement, however, decreased as the oxygen concentration was reduced and for sample C (x = 0.07) the intensity increased by only a factor of 1.8 ± 0.3. If , as was suggested by Friedl et al[41], it is assumed that the large enhancement occurs because of a near resonance between the phonon energy and the superconducting gap

energy, these results imply that the B_{1g} gap energy increases by about 90 ± 30 cm^{-1} as the oxygen concentration is reduced from 7.00 to 6.93. This result is in accord with:

(1) phonon anomaly measurements[35] which also imply an increase in the gap energy with decreasing oxygen concentration and

(2) direct measurements of the B_{1g} continuum which reveal an $80cm^{-1}$ shift of the peak frequency to higher energies as the oxygen concentration is reduced from 7.00 to 6.93.

It is thus concluded that the results obtained in this thesis, for both the A_{1g} and B_{1g} phonons, provide support for the applicability of the resonant mechanism proposed by Friedl et al.[41]

The onset temperature of the superconductivity induced intensity enhancement of the B_{1g} phonon has been found to be very close to the superconducting transition temperature T_c in all three samples studied in this work. This would indicate that the phonon is in resonance with the superconducting gap. The results also indicate, however, that the gap is anisotropic and that this anisotropy varies with oxygen concentration. That is the interpretation reqires that the B_{1g} gap be very sensitive to oxygen concentration while the A_{1g} gap is constant for $0 \leq x \leq 0.07$. Since the scattering is from excitations in the CuO_2 planes one could perhaps imagine that the shape of the Fermi surface might change rapidly with x and hence influence the gap in certain regions of k-space. However, photoemission experiments[37] have shown that the Fermi surface remains the same as the oxygen concentration in Y123 is varied. Thus this sensitivity to doping level

for $0 \leq x \leq 0.07$ is very difficult to explain if it is assumed that the B_{1g} phonon intensity enhancement arises from near resonance with a superconducting gap . In addition, previous calculations have shown that the A_{1g} continuum is well reproduced[38] given the existence of a d-wave gap, but the B_{1g} continuum is observed[38] to peak at a higher energy than is predicted. It has been suggested[68] that a screening mechanism could account for increased B_{1g} peak energy, but this yields[68] results which are in direct contrast to the observed[30] doping dependence. In conclusion the observed dependence of the gap anisotropy on oxygen concentration is not consistent with what one would expect for a superconducting gap. Thus it is suggested that the " gap " involved could arise from a different source as discussed in section 4.6.4 and the following section.

5.3 The Possible Relation between The B_{1g} Phonon Enhancement and A Spin Gap

In the resonant valence bond theory developed by Lee and Nagaosa[56,57], the opening of a spin gap is predicted for the underdoped materials at temperatures higher than T_c. All the energies involved there in the formation of a spin gap are on the scale of electronic energy, therefore the high transition temperature itself can be explained. The spin gap is dependent on the oxygen content. If the B_{1g} electronic continuum is related to scattering from spin fluctuations, then the sensitivity of the B_{1g} phonon anomaly and the intensity enhancement to oxygen content could be explained.

Both Raman[55,67] and Infrared[24-26] experiments carried out on

underdoped samples have revealed features that are consistent with a spin gap feature. For example, a Raman study found that the peak feature of the B_{1g} electronic continuum was established well above T_c in a sample with $x = 0.33$[55]. Another experiment found that the B_{1g} phonon anomaly occurred around 110K in a sample with $x = 0.05$[67]. All of the above factors have led us to speculate that the B_{1g} continuum arises at least in part from scattering from spin fluctuations and that the B_{1g} phonon is actually resonant with a spin gap.[56,57]

More work has to be done in order to definitely determine if the peak feature of the B_{1g} electronic continuum in the samples with low oxygen contents appears above T_c. If it does, it cannot be related to superconductivity. If it doesn't, it may be related to the superconducting gap. More work has also to be done to check if the B_{1g} phonon anomaly exists above T_c in the samples with low oxygen contents. This would provide a direct test of the spin gap proposed by Nagaosa and Lee.[56,57] In addition it would be interesting to study the intensity enhancement of the A_{1g} phonons for the (zz) or c-axis scattering geometry. Such measurements could provide information on the possible existence and nature of a c-axis gap which is presently[26,69] a somewhat controversial subject. There is still a long way to go to fully understand the superconducting mechanism in high-T_c materials.

References:

1. H. K. Onnes, Leiden Comm. 120 B, 122 B, 124C (1991).
2. V.D.Hunt, Superconductivity Sourcebook (John Wiley and Sons, 1989).
3. J.Bardeen, L.N.Cooper and J.R.Schrieffer, Phys. Rev. **108**, 1175(1957).
4. J.G.Bednorz and K.A.Muller, Z.Phys. B **64**, 189(1986).
5. M.K.Wu, J.R.Ashburn, C.J.Torng, P.H.Hor, R.L.Meng, L.Gao, Z.J.Huang, Y.Q.Wang and G.W.Chu. Phys. Rev. Lett. **58**, 908 (1987).
6. C.C.Torardi, M.A.Subramanian, J.C.Calabrese, J.Gopalakrishnan, K.J.Morrissey, T.R.Askew, R.B.Flippen, U.Chowdhry and A.M.Sleight, Science 240, 632(1988).
7. AShilling, M.Cantoni, J.D.Guo and H.R.Ott, Nature 363, 56(1993).
8. Y.Iye, Physical Properties of High Temperature Superconductors III, Edited by D.M.Ginsberg (World Scientific, 1992).
9. N.W.Ashcroft and N.D.Mermin, Solid State Physics, ch.26 (1976).
10. C.G.Olsen et al, Phys. Rev. B **42**, 381(1990).
11. B.Friedl, C.Thomsen and M.Cardona, Phys. Rev. Lett. **65**, 915(1990).
12. C.Thomson, M.Cardona, B.Friedl, C.O.Rodriguez, I.I.Mazin and O.K.Anderson, Solid State Commun. **75**, 219(1990).
13. M.V.Klein, Light Scattering in Solids, edited by M.Cardona, (Springer,1975).
14. S.B.Dierker, M.V.Klein, G.W.Webb and Z.Fisk, Phys. Rev. Lett. **50**, 853(1983).
15. M.V.Klein and S.B.Dierker, Phys. Rev. B **29**, 4976(1984).
16. R.Hackl, R.Kaiser and S.Schicktanz, J. Phys. C **16**, 1729 (1983).
17. L.A.Falkovsky and S.Klama, Physica C **172**, 242(1990).

18. R.Zeyher and G.Zwicknagl, Z. Phys. B- Condensed Matter **78**, 175(1990).

19. C.Thomsen, Light Scattering in Solid VI,(Springer- Verlag 1991).

20. D.B.Tanner and T.Timusk, Physical Properties of High Temperature Superconductors III, edited by D.M.Ginsberg(World Scientific, 1992).

21. A.P.Litvinchuk, C.Thomson and M.Cardona, preprint to appear in Physical Properties of High Temperature Superconductors IV. (World Scientific)

22. J.D.Axe and G.Shirane, Phys. Rev. B **8**, 1965(1973).

23. S.M.Shapiro, G.Shirane and J.D.Axe, Phys. Rev. B **12**, 4899(1975).

24. A.P.Litvinchuk, C.Thomson and M.Cardona, Solid State Commun. **83**, 343(1992).

25. A.P.Litvinchuk at al, preprint.

26. C.C.Homes, T.Timusk, R.Liang, D.A.Bonn and W.N.Hardy, Phys.Rev.Lett. **71**, 1645(1993).

27. D.Reznik, A.Kotz, S.L.Cooper, M.V.Klein,W.C.Lee and D.M.Ginsberg, Electronic Properties and Mechanism of High T_c Superconductors, 283 (Amsterdam Netherlands 1992).

28. D.Reznik, M.V.Klein, W.C.Lee and D.M.Ginsberg, Phys. Rev. B **46**, 11725 (1992).

29. A.A.Maksimov, A.V.Puchkov, I.I.Tartakovskii, D.Reznik, M.V.Klein, W.C.Lee and D.M.Ginsberg, JEPT Lett. **56**, 571(1992).

30. X.K.Chen, E.Altendorf, J.C.Irwin, R.Liang and W.N.Hardy, Phys. Rev. B **48**,10530(1993).

31. T.Staufer, R.Nemetschek, R.Hackl, P.Muller and H.Veith, Phys. Rev. Lett. **68**, 1069(1992).

32. V.B.Timofeev, A.A.Maksimov, O.V.Misochko and I.I.Tartakovskii, Physica C **162-164**,1409(1989).

33. S.L.Cooper, F.Slakey, M.V.Klein, J.P.Rice, E.D.Bukowski and D.M.Ginsberg, Phys. Rev. B **38**, 11934(1988).

34. S.L.Cooper, M.V.Klein, B.G.Pazol, J.P.Rice and D.M.Ginsberg, Phys. Rev. B**37**, 5920 (1988).

35. E.Altendorf, X.K.Chen, J.C.Irwin, R.Liang and W.N.Hardy, Phys. Rev. B **47**,8140(1993).

36. M.V.Klein, S.L.Cooper, A.L.Kotz, Ran Lin, D.Reznik, F.Slakey, W.C.Lee and D.M.Ginsberg, Physica C **185-189**, 72(1991).

37. R.Liu, B.W.Veal, A.P.Paulikas, J.W.Downey, P.J.Kosti, S.Fleshler, U.Wipp, C.G.Olson X.Wu, A.J.Arka and J.J.Joyce, Phys.Rev. B **46**, 11056(1992).

38. X.K.Chen, E.Altendorf, J.C.Irwin, R.Liang and W.N.Hardy, to be published.

39. E.T.Heyen, S.N.Rashkeev, I.I.Mazin, O.K.Anderson, R.Liu, M.Cardona and O.Jepsen, Phys. Rev. Lett. **65**, 3048 (1990)

40. O.V.Misochko, E.I.Rashba, E.Sherman and V.B.Timafeev, Phys. Reports **194**, 387 (1990).

41. B.Friedl, C.Thomsen, H-U. Habermerier and M.Cardona, Solid State Commun. **78**, 291(1991)

42. D.J.Gardiner, Practical Raman Spectroscopy, edited by D.J.Gardiner and P.R.Graves (Springer Verlag, 1989).

43. J.D.Jackson, Classical Electrodynamics, Ch. 9(1975).

44. A.Pinczuk and E.Burnstein, Light Scattering in Solids, edited by M.Cardona (Springer Verlag, 1983).

45. C.Thomsen and M.Cardona, Physical Properties of High Temperature Superconductors *I*, edited by D.M.Ginsberg (World Scientific, 1989).

46. D.L.Rousseau, R.P.Bauman and S.P.S.Porto, Journal of Raman Spectroscopy, **10**, 253(1981).

47. F.E.Bates, Phys. Rev. B **39**, 322(1989).

48. W.Kress, U.Schroder, J.Prade, A.D.Kulkarni and F.W. de Wette, Phys. Rev. B **38**, 2906(1988).

49. R.Liu, C.Thomsen, W.Kress, M.Cardona, B.Gegenheimer, F.W. de Wette, J.Prade, A.D.Kulkarni and U.Schroder, Phys. Rev. B **37**, 7971(1988).

50. C.O.Rodriguez, A.I.Liechtenstein, I.I.Mazin, O.Jepsen and O.K.Anderson, Phys.Rev.B **42**, 2692(1990).

51. K.F.McCarty, J.Z.Liu, R.N.Shelton and H.B.Radousky, Phys. Rev. B **41**, 8792(1990).

52. K.F.McCarty, H.B.Radousky. J.Z.Liu and R.N.Shelton, Phys. Rev. B **43**, 13751(1991).

53. B.Friedl, C.Thomsen, E.Schonher and M.Cardona, Solid State Commun. **76**, 1107 (1990).

54. C.Thomsen, M.Cardona, B.Gegenheimer,R.Liu and A.Simon, Phys. Rev. B **37**, 9860(1988).

55. F.Slakey, M.V.Klein, J.P.Rice and D.M.Ginsberg, Phys. Rev. B **42**, 2643(1990).

56. N.Nagaosa and P.A.Lee, Phys. Rev. B **45**, 966(1992).

57. P.A.Lee and N.Nagaosa, Phys. Rev. B **46**, 5621(1992).

58. R.Liang, P.Dosanjh, D.A.Bonn, D.J.Baar, J.F.Carolan and W.N.Hardy, Physica.C **195**, 51(1992).

59. E.Altendorf, J.C.Irwin, R.Liang and W.N.Hardy, Phys. Rev. B **45**, 7551(1992).

60. P.Monthoux, A.V.Balatsky and D.Pines, Phys. Rev. Lett. **67**,3448(1991).

61. W.N.Hardy, D.A.Bonn, D.C.Morgan, R.Liang and K.Zheng, Phys. Rev. Lett. **70**,3999(1993).

62. E.J.Nicol, C.Jiang and J.P.Carbotte, Phys. Rev. B**47**,8131(1993).

63. R.J.Birgeneau and G.Shirane, Physical Properties of High Temperature Superconductors, edited by D.M.Ginsberg(World Scientific,1989).

64. G.Shirane, J.Als-Nielsen, M.Nielsen, J.M.Tranquada, H.Chou, S.Shamoto and M.Sato, Phys. Rev. B **41**,6547(1990).

65. J.M.Tranquada, W.J.L.Buyers, H.Chou, T.E.Mason, M.Sato, S.Shamoto and G.Shirane, Phys. Rev. Lett. **64**, 800(1990).

66. A.P.Litvinchuk, C.Thomsen and M.Cardona, Solid State Commun. **80**, 257(1991).

67. G.Blumberg, L.Borjesson, R.Liang and W.N.Hardy, preliminary draft.

68. T.P.Devereaux, D.Einzel, B.Stadlober, R.Hackl, D.H.Leach and J.J.Neumeier, Phys. Rev. Lett. **72**, 396(1994).

69. M.Boekholt, M.Hoffmann and G.Guntherodt, Physica C **175**, 127(1991).